# Site U1302–U1308 methods[1]

Expedition 303 Scientists[2]

## Chapter contents

# Introduction

## Site locations

At all Integrated Ocean Drilling Program (IODP) Expedition 303 sites, Global Positioning System (GPS) coordinates from precruise site surveys were used to position the vessel on site. The only seismic system used during the cruise was the 3.5 kHz profiler, which was monitored on the approach to each site to compare the seismic characteristics of the sediments with those from the precruise survey. Once the vessel was positioned at a site, the thrusters were lowered and a reference beacon was deployed. Although the automated stationkeeping system of the vessel usually uses GPS data, the beacon provides a backup reference in case of problems with the transmission of satellite data. The final site position was the mean position calculated from the GPS data collected over the time the site was occupied.

## Drilling operations

One coring system was used during Expedition 303: the advanced piston corer (APC). The APC is a "cookie-cutter" system that cuts cores with minimal coring disturbance. The drill pipe is pressured up until the failure of one or two shear pins that hold the inner barrel to the outer barrel. The inner barrel strikes out and cuts the core. The driller can detect a successful cut, or "full stroke," on the pressure gauge on the rig floor.

The standard bottom-hole assembly used at all Expedition 303 sites was composed of an 11$\frac{7}{16}$ inch rotary bit, a bit sub, a seal bore drill collar, a landing saver sub, a modified top sub, a modified head sub, a nonmagnetic drill collar, five 8¼ inch drill collars, a tapered drill collar, six joints of 5½ inch drill pipe, and one crossover sub. A lockable float valve was used instead of the standard float assembly if the possibility of logging existed. APC refusal is conventionally defined in two ways: (1) the piston fails to achieve a complete stroke (as determined from the pump pressure reading) because the formation is too hard, and (2) excessive force (>60 klb) is required to pull the core barrel out of the formation. In cases where full stroke can be achieved but excessive force cannot retrieve the barrel, the core barrel can be "drilled over" (i.e., after the inner core barrel is successfully shot into the formation, the rotary bit is advanced to total depth to free the APC barrel). This strategy allows a hole to be advanced much farther with the APC, the preferred coring tool. A total of 46 core barrels were

drilled over during Expedition 303. Nonmagnetic core barrels were used during all conventional APC coring. When using the drillover technique, standard steel core barrels were used because they are more robust and less costly to replace if damaged

Each cored interval was ~9.5 m long, which is the length of a core barrel. In some cases, the drill string was drilled or "washed" ahead without recovering sediments to advance the drill bit to a target depth where we needed to resume core recovery. Such advances were necessary in multiple holes per site to ensure that coring gaps in one hole were covered by cored intervals in adjacent holes. The amount of advance was typically 1–4 m and accounted for drilling depth shift caused by tides, heave, and other factors (see "Composite section"). Drilled and cored intervals are referred to in meters below rig floor (mbrf), which are measured from the dual elevator stool (DES) on the rig floor to the bottom of the drill pipe. In cases where sediments of substantial thickness cover the seafloor (as at all sites during Expedition 303), the mbrf depth of the seafloor is determined with a mudline core, assuming 100% recovery for the cored interval in the first core. If the first core recovered a full barrel of sediment (it "missed the mudline"), the seafloor reference depth of a previous or later hole was used. Water depth was calculated by subtracting the distance between the DES and sea level (typically 10–11 m, depending on the ship's load at a given time) from the mbrf depth. The water depth determined in this way (drill string measurement) usually differs from precision depth recorder measurements by a few to several meters. The meters below seafloor (mbsf) depths of core tops are calculated by subtracting the seafloor depth in mbrf from the core-top depth in mbrf. The core-top datums from the driller are the ultimate depth reference for any further depth calculation procedures.

## Core handling and analysis

As soon as cores arrived on deck, gas void samples were taken for immediate analysis as part of the shipboard safety and pollution prevention program. Core catcher samples were taken for biostratigraphic analysis. When the core was cut in sections, whole-round samples were taken for shipboard interstitial water examinations. In addition, headspace gas samples were immediately taken from the ends of cut sections and sealed in glass vials for light hydrocarbon analysis.

Before the cores were split, whole-round core sections were run through the multisensor track (MST) and thermal conductivity measurements were taken. In addition, whole cores were run through a mag-

netic susceptibility (MS) core logger (MSCL; also known as the "Fast Track"), originally equipped with two magnetic susceptibility loops but later reduced to one (see "Physical properties") to facilitate real-time drilling decisions to maximize stratigraphic overlap between holes (see "Composite section"). The cores were then split into working and archive halves, from bottom to top, so investigators should be aware that older material could have been transported upward on the split face of each section. The working half of each core was sampled for both shipboard analysis (i.e., physical properties, carbonate, and bulk X-ray diffraction mineralogy) and shore-based studies. Shipboard sampling was kept at a minimum during Expedition 303 to allow construction of a detailed sampling plan after the composite section was built (see "Composite section"). The archive-half sections were scanned on the digital imaging system (DIS), measured for color reflectance on the archive multisensor track (AMST), described visually and by means of smear slides, run through the cryogenic magnetometer, and finally photographed with color film a whole core at a time. Digital close-up photographs were taken of particular features for illustrations in site reports, as requested by scientists. Both halves of the core were then put into labeled plastic tubes, sealed, and transferred to cold storage space aboard the ship. At the end of the expedition, the cores were transferred from the ship into refrigerated trucks and to cold storage at the IODP Bremen Core Repository in Bremen, Germany.

## Curatorial procedures and sample depth calculations

Numbering of sites, holes, cores, and samples followed the standard IODP procedure. A full curatorial identifier for a sample consists of the following information: expedition, site, hole, core number, core type, section number, and interval in centimeters measured from the top of the core section. For example, a sample identification of "303-U1302A-1H-1, 10–12 cm" represents a sample removed from the interval between 10 and 12 cm below the top of Section 1 of Core 1 (H designates that this core was taken with the APC system) of Hole U1302A during Expedition 303. The "U" preceding site or hole designates site/holes drilled by the IODP riserless vessel. Cored intervals are also referred to in "curatorial" mbsf. The mbsf of a sample is calculated by adding the depth of the sample below the section top and the lengths of all higher sections in the core to the core-top datum measured with the drill string. A soft to semisoft sediment core from less than a few hundred meters below seafloor expands upon recovery

(typically 10%–15%), so the recovered interval does not match the cored interval. In addition, a coring gap typically occurs between cores, as shown by composite depth construction (see "Composite section") (i.e., some cored interval was lost during recovery or was never cut). Thus, a discrepancy exists between the drilling mbsf and the curatorial mbsf. For instance, the curatorial mbsf of a sample taken from the bottom of a core is larger than that of a sample from the top of the subsequent core, where the latter does correspond to the drilled core-top datum. During Expedition 303, multiple APC holes were drilled at a site to construct a continuous composite section. This resulted in a "meters composite depth (mcd)" scale for each site that accommodates core expansion and drilling gaps through interhole correlation of closely spaced measurements of core physical properties (see "Composite section").

# Lithostratigraphy

This section outlines the procedures followed to document the basic sedimentology of the deposits recovered during IODP Expedition 303, including core description, X-ray diffraction (XRD) studies, color spectrophotometry, and smear slide description. Only general procedures are outlined, except where they depart significantly from Ocean Drilling Program (ODP) and IODP conventions.

## Sediment classification

The sediments recovered during Expedition 303 were composed of biogenic and siliciclastic components. They were described using the classification scheme of Mazzullo et al. (1988). The biogenic component is composed of the skeletal debris of open-marine calcareous and siliceous microfauna (e.g., foraminifers and radiolarians, respectively) and microflora (e.g., calcareous nannofossils and diatoms, respectively) and associated organisms. The siliciclastic component is composed of mineral and rock fragments derived from igneous, sedimentary, and metamorphic rocks. The relative proportions of these two components are used to define the major classes of "granular" sediments in the scheme of Mazzullo et al. (1988).

The lithologic names assigned to these sediments consist of a principal name and modifiers based on composition and degree of lithification and/or texture as determined from visual description of the cores and from smear slide observations. The total calcium carbonate content of the sediments, determined on board (see "Sedimentary inorganic and organic carbon, nitrogen, and sulfur concentrations" in "Geochemistry"), also aided in classifica-

tion. For a sediment that is a mixture of components, the principal name is preceded by major modifiers (in order of increasing abundance) that refer to components making up >25% of the sediment. Minor components that represent between 10% and 25% of the sediment follow the principal name (after "with") in order of increasing abundance. For example, an unconsolidated sediment containing 30% nannofossils, 25% clay minerals, 20% foraminifers, 15% quartz silt, and 10% manganese nodules would be described as a clayey nannofossil ooze with manganese nodules, quartz silt, and foraminifers. Although these minor sedimentary components, ranging in abundance from 10% to 25%, are reflected in the sediment name in the description column as "with," these components are not designated in the Graphic Lithology column of the barrel sheets.

These naming conventions follow the ODP sediment classification scheme (Mazzullo et al., 1988), with the exception that a separate "mixed sediment" category was not distinguished during Expedition 303 (Fig. F1). As a result, biogenic sediments are those that contain >50% biogenic grains and <50% siliciclastic grains, whereas siliciclastic sediments are those that contain >50% siliciclastic grains and <50% biogenic grains. During Expedition 303, neritic and chemical sediments were not encountered except as accessory components; therefore, these categories are not addressed below. Sediments containing >50% silt- and sand-sized volcanic grains were classified as ash layers. Size divisions for siliciclastic grains are those of Wentworth (1922) (Fig. F2), with 10 major textural categories defined on the basis of the relative proportions of sand, silt, and clay (Fig. F3); however, distinguishing between some of these categories is difficult (e.g., silty clay versus clayey silt) without accurate measurements of grain size abundances. The term "clay" is only used to describe particle size and is applied to both clay minerals and other siliciclastic material <4 µm in size. Size-textural qualifiers were not used for biogenic sediment names (e.g., nannofossil clay implies that the dominant component is detrital clay rather than clay-sized nannofossils).

Terms that describe lithification vary depending on the dominant composition as described below:

- Sediments composed predominantly of calcareous, pelagic organisms (e.g., calcareous nannofossils and foraminifers): the lithification terms "ooze" and "chalk" reflect whether the sediment can be deformed with a finger (ooze) or can be scratched easily by a fingernail (chalk).

- Sediments composed predominantly of siliceous microfossils (diatoms, radiolarians, and siliceous sponge spicules): the lithification terms "ooze"

and "radiolarite/spiculite/diatomite" reflect whether the sediment can be deformed with a finger (ooze) or cannot be easily deformed manually (radiolarite/spiculite/diatomite).

- Sediments composed predominantly of siliciclastic material: if the sediment can be deformed easily with a finger, no lithification term is added and the sediment is named for the dominant grain size (e.g., "clay"). For more consolidated material, the lithification suffix "-stone" is appended to the dominant size classification (e.g., "claystone").

- Sediments composed of sand-sized volcaniclastic grains: if the sediment can be deformed easily with a finger, the interval is described as ash. For more consolidated material, the rock is called tuff.

## Visual core description

### Preparation for core description

The standard method of splitting a core by pulling a wire lengthwise through its center tends to smear the cut surface and obscure fine details of lithology and sedimentary structure. When necessary during Expedition 303, the archive halves of cores were gently scraped across, rather than along, the core section using a stainless steel or glass scraper to prepare the surface for unobscured sedimentologic examination and digital imaging. Scraping parallel to bedding with a freshly cleaned tool prevented cross-stratigraphic contamination.

### Sediment barrel sheets

Core-description forms, or "barrel sheets," provide a summary of the data obtained during shipboard analysis of each sediment core. Detailed observations of each section were initially recorded by hand on standard IODP visual core description (VCD) forms. Copies of original VCD forms are available from IODP upon request. This information was subsequently entered into AppleCORE software (version 9.4), which generates a simplified, annotated graphical description (barrel sheet) for each core (Fig. **F4**). Site, hole, and depth (in mbsf or mcd, if available) are given at the top of the barrel sheet, with the corresponding depths of core sections along the left margin. Columns on the barrel sheets include Graphic Lithology, Bioturbation, Structures, Accessory Components, Sediment Disturbance, Sample Types, Color, and Remarks. These columns are discussed in more detail below.

### Graphic lithology

Lithologies of the core intervals recovered are represented on barrel sheets by graphic patterns in the column titled Graphic Lithology, using the symbols

illustrated in Figure **F5.** A maximum of two different lithologies (for interbedded sediments) or three different components (for a uniform sediment) can be represented within the same core interval. Minor lithologies, present as thin interbeds within the major lithology, are shown by a dashed vertical line dividing the lithologies. Lithologic abundances are rounded to the nearest 10%; lithologies that constitute <10% of the core are generally not shown but are listed in the Description section. However, some distinctive minor lithologies, such as ash layers, are included graphically in the lithology column. Contact types (e.g., sharp, scoured, and gradational) are also shown in the Graphic Lithology column. Relative abundances of lithologies reported in this way are useful for general characterization of the sediment but do not constitute precise, quantitative observations.

### Bioturbation

Five levels of bioturbation are recognized using a scheme similar to that of Droser and Bottjer (1986). Bioturbation intensity is classified as abundant (>75%), common (>50%–75%), moderate (10%–50%), rare (<10%), and absent (none). These levels are illustrated with graphic symbols in the Bioturbation column (Fig. **F6**).

### Sedimentary structures

The locations and types of sedimentary structures visible on the prepared surfaces of the split cores are shown in the Structure column of the core description form. Symbols in this column indicate the locations of individual bedding features and any other sedimentary features, such as scours, ash layers, ripple laminations, and fining-upward or coarsening-upward intervals (Fig. **F6**).

### Accessory components

Lithologic, diagenetic, and paleontologic accessories, such as nodules, sulfides, and shells, are indicated on the barrel sheets. The symbols used to designate these features found in Expedition 303 sediments are shown in Figure **F6.**

### Sediment disturbance

Drilling-related sediment disturbance that persists over intervals of ≥20 cm is recorded in the Disturbance column using the symbols shown in Figure **F6.** The degree of drilling disturbance is described for soft and firm sediments using the following categories:

- Slightly disturbed: bedding contacts are slightly deformed.

- Moderately disturbed: bedding contacts have undergone extreme bowing.
- Highly disturbed: bedding is completely deformed as flow-in, coring/drilling slurry, and other soft sediment stretching and/or compressional shearing structures attributed to coring/drilling. The particular type of deformation may also be noted (e.g., flow-in, gas expansion, etc.).
- Soupy: intervals are water saturated and have lost all aspects of original bedding.

## Sample types

Sample material taken for shipboard sedimentologic and chemical analyses consisted of pore water whole rounds, micropaleontology samples, smear slides, and discrete samples for XRD. Typically, one to five smear slides were made per core, one pore water sample was taken at a designated interval, and a micropaleontology sample was obtained from the core catcher of most cores. XRD samples were taken only where needed to assess the lithologic components. Additional samples were selected to better characterize lithologic variability within a given interval. Tables summarizing relative abundance of sedimentary components from the smear slides were also generated.

## Color

Color is determined qualitatively using Munsell Soil Color Charts (Munsell Color Company, Inc., 1994) and described immediately after cores are split to avoid color changes associated with drying and redox reactions. When portions of the split core surface required cleaning with a stainless steel or glass scraper, this was done prior to determining the color. Munsell color names are provided in the Color column on the barrel sheet, and the corresponding hue, value, and chroma data are provided with the Remarks.

## Remarks

The written description for each core contains a brief overview of both major and minor lithologies present and notable features such as sedimentary structures and disturbances resulting from the coring process.

## Smear slides

Smear slide samples were taken from the archive halves during core description. For each sample, a small amount of sediment was removed with a wooden toothpick, dispersed evenly in deionized water on a 1 inch × 3 inch glass slide, and dried on a hot plate at a low setting. A drop of mounting medium and a 1 inch × 1 inch cover glass was added, and the slide was placed in an ultraviolet light box for ~30 min. Once fixed, each slide was scanned at 100×–200× with a transmitted light petrographic microscope using an eyepiece micrometer to assess grain-size distributions in clay (<4 μm), silt (4–63 μm), and sand (>63 μm) fractions. The eyepiece micrometer was calibrated once for each magnification and combination of ocular and objective, using an inscribed stage micrometer.

Relative proportions of each grain size and type were estimated by microscopic examination. Note that smear slide analyses tend to underestimate the abundance of sand-sized and larger grains (e.g., foraminifers, radiolarians, and siliciclastic sand) because these are difficult to incorporate into the smear. Clay-sized biosilica, being transparent and isotropic, is also very difficult to quantify. Clay minerals, micrite, and nannofossils can also be difficult to distinguish at the very finest (less than ~4 μm) size range. After scanning for grain-size distribution, several fields were examined at 200×–500× for mineralogical and microfossil identification. Standard petrographic techniques were employed to identify the commonly occurring minerals and biogenic groups, as well as important accessory minerals and microfossils.

Smear slide analysis data tables are included in **"Core descriptions."** These tables include information about the sample location, whether the sample represents a dominant (D) or a minor (M) lithology in the core, and the estimated percentages of sand, silt, and clay, together with all identified components.

## Abundance of gravel-sized grains

One of the primary objectives of Expedition 303 was to collect cores that record the paleoclimatic history of the North Atlantic at millennial and longer timescales. Because of the geographic location and the geologic age of these sediments, ice-rafted debris (IRD) was expected to be an important part of that paleoclimatic record. The most easily identified IRD consists of outsized clasts in a fine-grained pelagic matrix and is often defined operationally as gravel-sized grains. During Expedition 303, the abundance of IRD was estimated by counting the number of gravel-sized grains (i.e., granule size and larger) in each 10 cm increment of the core. These counts were recorded and reported in tables that are available upon request from the IODP Data Librarian. The presence and composition of larger clasts (pebble size and larger) was noted.

## Spectrophotometry (color reflectance)

Reflectance of visible light from the surface of split sediment cores was routinely measured using a Minolta spectrophotometer (model CM-2002) mounted on the AMST. The AMST measures the archive half of each core section and provides a high-resolution stratigraphic record of color variations for visible wavelengths (400–700 nm). Freshly split soft cores were covered with clear plastic wrap and placed on the AMST. Measurements were taken at 2.0 cm spacing. The AMST skips empty intervals and intervals where the core surface is well below the level of the core liner, but does not skip relatively small cracks, disturbed areas of core, or large clasts. Thus, AMST data may contain spurious measurements, which should be edited out of the data set. Each measurement recorded consists of 31 separate determinations of color reflectance in 10 nm wide spectral bands from 400 to 700 nm. Additional detailed information about measurement and interpretation of spectral data with the Minolta spectrophotometer can be found in Balsam et al. (1997, 1998) and Balsam and Damuth (2000).

## X-ray diffraction analysis

Selected samples were taken for qualitative mineral analysis by using an XRD Philips model PW1729 X-ray diffractometer using Ni-filtered $CuK_\alpha$ radiation. Instrument conditions were as follows: 40 kV, 35 mA; goniometer scan from 2° to 70°2θ (air-dried samples); step size of 0.01°2θ; and count time of 1 s each. MacDiff software (version 4.1.1 PPC by Rainer Petschick) was used to display diffractograms, and identifications are based on multiple peak matches, using the mineral database provided with MacDiff.

## Digital color imaging

Systematic, high-resolution, line-scan digital core images of the archive half of each core were obtained using the Geotek X-Y imaging system (Geoscan II). This DIS collects digital images with three line-scan charge-coupled device arrays (1024 pixels each) behind an interference filter to create three channels (red, green, and blue). The image resolution is dependent on the width of the camera and core. The standard configuration for Geoscan II produces 300 dpi on an 8 cm wide core with a zoom capability up to 1200 dpi on a 2 cm wide core. Synchronization and track control are better than 0.02 mm. The dynamic range is 8 bits for all three channels. The framestore card has 48 MB of onboard random access memory for the acquisition of images with an ISA interface card for personal computers. After cores were visually described, they were placed in the DIS

and scanned. A spacer holding a neutral gray color chip and a label identifying the section was placed at the base of each section and scanned along with each section. Output from the DIS includes a Windows bitmap (.BMP) file and a JPEG (.JPG) file for each section scanned. The bitmap file contains the original data. Additional postprocessing of data was done to achieve a medium-resolution JPEG image of each section and a composite JPEG image of each core, which is comparable to the traditional photographic image of each core. The JPEG image of each section was produced by an Adobe Photoshop batch job that opened the bitmap file, resampled the file to a width of 0.6 inches (~15 mm) at a resolution of 300 pixels/inch, and saved the result as a maximum-resolution JPEG. The DIS system was calibrated for black and white approximately every 12 h. No significant change in this calibration was observed during Expedition 303. A constant aperture setting of f/11 was used.

# Biostratigraphy

Preliminary ages were assigned based primarily on core catcher samples. Samples from within the cores were examined when a more refined age determination was necessary. Ages for calcareous nannofossil, foraminiferal, diatom, radiolarian, and palynological events in the late Miocene to Quaternary were estimated by correlation to the geomagnetic polarity timescale (GPTS) of Cande and Kent (1995). Biostratigraphic events, zones, and subzones for nannofossils, planktonic foraminifers, and diatoms are summarized in Figure F7. The Pliocene/Pleistocene boundary has been formally located just above the top of Olduvai (C2n) magnetic polarity subchron (Aguirre and Pasini, 1985) and just below the first occurrence (FO) of *Gephyrocapsa caribbeanica* (Takayama and Sato, 1993–1995). We used the FO of *G. caribbeanica* to mark the Pliocene/Pleistocene boundary. The Miocene/Pliocene boundary has not yet been formally defined. We tentatively used the last occurrence (LO) horizon of *Discoaster quinqueramus* for the boundary. The FOs of *Globorotalia margaritae* (planktonic foraminifer) and *Thalassiosira convexa* (diatom) also mark the approximate position of the stage boundary. Details of the shipboard methods are described below for each microfossil group.

## Calcareous nannofossils

The zonal scheme established by Martini (1971) was used for upper Miocene to Quaternary sequences during Expedition 303. In addition, the Upper Pliocene–Quaternary biohorizons defined by Sato et al. (1999) were used for more detailed correlations.

Age estimates for all upper Miocene–Quaternary datums were based on and correlated to the GPTS of Cande and Kent (1995). These zonal scheme and nannofossil biohorizons are shown in Figure F7.

## Methods

Standard smear slide methods were used for all samples, using Norland optical adhesive as a mounting medium. Calcareous nannofossils were examined under a light-polarizing microscope at 1250× magnification.

We followed the taxonomic concepts summarized in Takayama and Sato (1987; Deep Sea Drilling Project Leg 94). Calcareous nannofossil preservation was assessed as follows:

G = good (little or no evidence of dissolution and/ or overgrowth).

M = moderate (minor dissolution or crystal overgrowth observed).

P = poor (strong dissolution or crystal overgrowth, many specimens unidentifiable).

The total abundance of calcareous nannofossils for each sample was estimated as follows:

A = very abundant (>50 specimens/field of view).

C = common (10–50 specimens/field of view).

F = few (1–10 specimens/field of view).

R = rare (1 specimen/2 or more fields of view).

Nannofossil abundances of individual species were recorded as follows:

A = abundant (1–10 specimens/field of view).

C = common (1 specimen/2–10 fields of view).

R = rare (1 specimen/>10 fields of view).

## Foraminifers

Preliminary ages were assigned based on the presence of planktonic foraminifers in core catcher samples. The zonal schemes of Weaver and Clement (1987) were applied to the late Neogene and Quaternary samples of Expedition 303 (Fig. F7). Because FOs and LOs of planktonic foraminifers are diachronous across the temperate to subpolar North Atlantic (Weaver and Clement, 1987; Spencer-Cervato and Thierstein, 1997), we did not assign absolute ages to these occurrences. Taxonomic concepts for Neogene taxa were adopted from Kennett and Srinivasan (1983).

Benthic foraminifers provide limited biostratigraphic age control as currently applied to Expedition 303 samples. The LO of the benthic foraminifer *Stilostomella* was noted whenever possible. Most *stilostomella* species disappeared from the global ocean at different latitudes during the interval of 1.0–0.6 Ma (Hayward, 2001). Taxonomic assignments on the ge-

neric level follow Loeblich and Tappan (1988). Benthic foraminifers were identified mainly to determine past changes in hydrography and surface water productivity. Oxygenation and carbon flux are the main factors controlling abundance and species composition in deep-sea assemblages (Jorissen et al., 1995; Altenbach et al., 2003).

## Methods

From each core catcher, 10 cm³ of sediment was analyzed for planktonic and benthic foraminifers. Unlithified sediment samples were soaked in tap water and then washed over a 63 μm sieve. Semilithified material was soaked in a 3% $H_2O_2$ solution before washing. Washed samples were dried at 60°C and analyzed under a Zeiss Stemi SV 11 binocular microscope. Planktonic and benthic foraminifers were analyzed from the same residues. Cleaned sieves were put into a sonicator for several minutes to avoid contamination between successive samples.

Planktonic foraminiferal abundance in relation to total residue was categorized as follows:

A = abundant (>50%).

C = common (10%–50%).

R = rare (<10%).

B = barren.

Preservation was categorized as follows:

VG = very good (no evidence of breakage or dissolution).

G = good (dissolution effects are rare; >90% of specimens unbroken).

M = moderate (dissolution damages, such as etched and partially broken tests, occur frequently; 30%–90% of specimens unbroken).

P = poor (strongly recrystallized or dominated by fragments or corroded specimens).

Planktonic foraminiferal species abundance in a random sample of 100–300 specimens from the >63 μm size fraction was defined as follows:

D = dominant (>30%).

A = abundant (10%–30%).

F = few (5%–10%).

R = rare (1%–5%).

P = present (<1%).

## Diatoms

The Neogene and Quaternary diatom zonation used for the high-latitude sites of Expedition 303 was that earlier proposed by Baldauf (1985) and Koç et al. (1999) (Fig. F7). The late Miocene–Holocene part of these zonations is based on the presence of a warm-temperature diatom assemblage in the North Atlantic similar to that recorded from the eastern equato-

rial Pacific (Burckle, 1972, 1977; Baldauf, 1985; Barron, 1985).

Typical diatom assemblages preserved in the sedimentary record can be used as tracers of the corresponding hydrographic conditions of the surface waters. Abundant diatoms characterize fertile surface waters of high latitudes and coastal upwelling areas. In the North Atlantic north of ~50°N, diatom assemblages are species rich and are the main contributors to the biogenic silica preserved in the sediment (Baldauf, 1985; Koç et al., 1999).

## Methods

Two types of slides were prepared for diatom analysis, depending on overall abundance. For areas of high abundance, smear slides were prepared from a small amount of raw material in a core catcher. At a low concentration of diatom valves and/or abundant clay, selected core catcher samples were boiled in a solution of $H_2O_2$ and sodium pyrophosphate to remove organic matter and to disperse the clay-sized material, followed by treatment with hydrochloric acid to remove $CaCO_3$. The treated samples were then washed several times with distilled water. In each case, aliquots of raw and cleaned samples were mounted on microslides using Norland optical adhesive. All slides were examined with phase-contrast illumination at a magnification of 1000× for stratigraphic markers and paleoenvironmentally sensitive taxa. The counting convention of Schrader and Gersonde (1978) was adopted. Overall diatom abundance and species-relative abundances were determined based on smear slide evaluation, using the following convention:

- A = abundant (>100 valves/microslide traverse).
- C = common (40–100 valves/microslide traverse).
- F = few (20–40 valves/microslide traverse).
- R = rare (10–20 valves/microslide traverse).
- T = trace (<10 valves/microslide traverse).
- B = barren (no diatoms in sample).

Preservation of diatoms was determined qualitatively as follows:

- G = good (weakly silicified forms present and no alteration of frustules observed).
- M = moderate (weakly silicified forms present, but with some alteration).
- P = poor (weakly silicified forms absent or rare and fragmented, and the assemblage is dominated by robust forms).

## Radiolarians

Radiolarian biostratigraphy during Expedition 303 was based on the radiolarian zonation documented by Goll and Bjørklund (1989). Primary datums from the late Miocene–Pleistocene are listed in Table **T1.**

## Methods

Core catcher samples were treated with a 5%–8% solution of hydrochloric acid to dissolve all calcareous components. The solution was sieved through a 63 μm mesh screen. The residue was disaggregated by gentle boiling in a 5%–8% hydrogen peroxide solution and a few grams of Calgon and sieved again. The dried residue was divided equally by a simple splitter into smaller aliquots to obtain an appropriate number of specimens for a slide. One aliquot of residue was randomly scattered on a slide on which thin gum tragacanth was spread. A few drops of Norland optical adhesive were added to the strewn-slide and a 22 mm × 40 mm glass coverslip applied.

Overall radiolarian abundances were determined based on strewn-slide evaluation at 20× objective lens, using the following convention:

- A = abundant (>100 specimens/slide traverse).
- C = common (51–100 specimens/slide traverse).
- F = few (11–50 specimens per slide traverse).
- R = rare (1–10 specimens per slide traverse).
- T = trace (<1 specimens per slide traverse).
- B = barren (no radiolarians in sample).

The abundance of individual species was recorded relative to the fraction of the total assemblages as follows:

- A = abundant (>10% of the total assemblage).
- C = common (5%–10% of the total assemblage).
- F = few (<5% of the total assemblage).
- R = rare (a few or more specimens per slide).
- T = trace (present in slide).

Preservation was recorded as follows:

- G = good (majority of specimens complete, with minor dissolution, recrystallization, and/or breakage).
- M = moderate (minor but common dissolution, with a small amount of breakage of specimens).
- P = poor (strong dissolution, recrystallization, or breakage, many specimens unidentifiable).

## Palynology: dinoflagellate cysts, pollen, and other palynomorphs

Palynological sample preparations yielded several types of organic-walled microfossils (i.e., palynomorphs). They included mainly dinoflagellate cysts (dinocysts), pollen, and spores from terrestrial plants and organic linings of benthic foraminifers. In some marine environments, phycoma of prasinophyte algae and acritarchs are also recovered. During this ex-

pedition, we were looking at all palynomorphs, but more attention was paid to dinocysts as paleoecological and biostratigraphic indicators.

No calibrated zonal schemes have been established based on dinocysts for the Neogene interval. Nevertheless, many studies during the last decades have documented the late Cenozoic stratigraphic distribution of organic-walled dinocysts at several locations at middle to high latitudes in the North Atlantic Ocean. Regional schemes are available for Baffin Bay (Head et al., 1989a; de Vernal and Mudie, 1989a; Piasecki, 2003), the Labrador Sea (Head et al., 1989b; de Vernal and Mudie, 1989b, 1992), the Greenland Sea (Matthiessen and Brenner, 1996; Poulsen et al., 1996), the Norwegian Sea (Mudie, 1989; Manum et al., 1989), and the North Sea area (Head, 1998a, 1998b; Head et al., 2004; Louwye et al., 2004), in addition to a few other locations in the North Atlantic (e.g., Harland, 1979; Mudie, 1987; Powell, 1988; de Vernal et al., 1992; Head and Norris, 2003; Head and Westphal, 1999). Encountered dinocyst events were compared with these previous investigations and with the broad-scale succession of events and zones established by Powell (1992) and Williams et al. (1998).

## Methods

Approximately 5 cm³ of sample was processed using a simplified palynological treatment, avoiding HF treatments. The procedures included ultrasonic treatment, sieving on a 106 µm mesh sieve to discard coarse material, and sieving at 10 µm to eliminate clay and fine silt particles. The fraction between 15 and 106 µm was treated with HCl (10%) to remove carbonates. The residue was then submitted to differential settling in water. In some cases, heavy liquid separation with polytungstate solution was needed. In many cases, ultrasonic treatments were needed to deflocculate clays. Residues were sieved again over a 10 µm mesh sieve and mounted between slides and cover-slides with glycerine jelly.

Tablets of *Lycopodium* spores were included in the sample at the beginning of the preparation to allow a semiquantitative concentration calculation.

The slides were examined on a Zeiss Axioplan microscope equipped with differential interference contrast with magnification ranging from 250× to 630×. Taxonomic identifications were verified at 1000× magnification.

Abundance of each palynomorph group (i.e., dinocysts, pollen, spores, etc.) was calculated from relative proportions of the *Lycopodium* spores after scanning the slides. Abundances are reported as follows:

XXXX = extremely abundant (>10,000/cm³)
XXX = abundant (>1000/cm³).
XX = common (100–1000/cm³).
x = few (10–100/cm³).
r = rare (<10/cm³).

Special attention was given to dinocysts, which were counted and identified to the species level when possible. The relative abundance of taxa was defined as follows:

XXX = dominant (>30%).
XX = abundant (10%–30%).
x = few (2%–10%).
r = rare (<2%).

When counts were too low (<50 specimens) for percentage calculation, only the presence of specimens (P) and the observation of single specimen (o) are reported. Preservation of dinocysts, and palynomorphs in general, was determined qualitatively. It is reported as follows:

G = good (no trace of alteration of the organic walls; pollen and dinocysts spherical; occurrence of the least resistant taxa).
M = moderate (subtle indication of alteration, flattening palynomorphs; specimen occasionally broken).
P = poor (only most resistant palynomorph present, showing strong alteration features and flattering; specimens often broken).

# Paleomagnetism

Paleomagnetic studies aboard the *JOIDES Resolution* during Expedition 303 were composed of routine measurements of the natural remanent magnetization (NRM) of archive-half sections before and after alternating-field (AF) demagnetization and low-field volumetric magnetic susceptibility measurements made on whole cores.

Remanence measurements and AF demagnetizations were performed using a long-core cryogenic magnetometer (2G Enterprises model 760-R). This instrument is equipped with direct-current superconducting quantum interference devices (DC-SQUID) and has an inline AF demagnetizer capable of reaching peak fields of 80 mT. The spatial resolution measured by the width at half-height of the pickup coils response is <10 cm for all three axes, although they sense a magnetization over a core length up to 30 cm. The magnetic moment noise level of the cryogenic magnetometer is ~$10^{-4}$ Am². The practical noise level, however, is affected by the magnetization of the core liner and the background magnetization of the measurement tray, and magnetizations of ~5 × $10^{-5}$ A/m can be reliably measured.

The remanent magnetization of archive halves of all core sections was measured unless precluded or made worthless by drilling-related deformation. Measurements were made at intervals of 5 cm starting at 15 cm above and ending at 15 cm below the base of each section. The number of demagnetization steps and the peak field used reflected the demagnetization characteristics of the sediments, the severity of the drill string magnetic overprint, the desire not to exceed peak fields of 20 mT shipboard, and the need to maintain core flow through the laboratory. One step of three axes AF demagnetization and subsequent section measurement at 5 cm intervals takes ~5 min. Only 3 min are needed for measurement without AF demagnetization. Following NRM measurement, one-step demagnetization and measurement using peak fields of 10 or 20 mT was typically employed (~8 min). If time allowed or the drill string magnetic overprint was not removed, additional steps were added up to 20 mT. Low peak demagnetization peak fields ensure that archive halves remain useful for shore-based high-resolution (U-channel) studies of magnetic remanence.

Measurements were undertaken using the standard IODP magnetic coordinate system (+x = vertical upward from the split surface of archive halves, +y = left-hand split surface when looking upcore, and +z = downcore). Data were stored using the standard IODP file format. Data were manually checked for quality and the auto-save option was not used. The sample interval was set to 5 cm, leader and trailer lengths were both set to 15 cm, and no drift correction was applied. The program options for skipping voids and gaps at the top of the section were not used. Instead, void depths and otherwise disturbed intervals were manually noted on the "cryomag log sheets" and later taken into account. All sections were measured using an internal diameter setting of 6.5 cm. Background tray magnetization was measured at the beginning of each shift and subtracted from all measurements.

During APC coring, a nonmagnetic "monel" core barrel was used for all but some overdrilled parts of the section (see **"Drilling operations"** in "Introduction"). The low levels of drilling-related magnetic overprint can be attributed to the use of nonmagnetic core barrels. Full orientation was attempted using the Tensor (orientation) tool beginning at Core 3 of all holes. The Tensor tool is rigidly mounted onto a nonmagnetic sinker bar attached to the top of the core-barrel assembly. The Tensor tool consists of three mutually perpendicular magnetic-field fluxgate sensors and two perpendicular gravity sensors. The information from both sets of sensors allows the azimuth and dip of the hole to be measured as well as

azimuth of the APC core. The azimuthal reference line is the double orientation line on the core liner and remains on the working half after the core is split.

Where the shipboard AF demagnetization appeared to have isolated the characteristic remanent magnetization, paleomagnetic inclinations and/or declinations of the highest demagnetization step (typically 10 or 20 mT) were used to make an initial designation of magnetic polarity zones. The timescale of Cande and Kent (1995) with updated age estimates for the Cobb Mountain (Channell et al., 2002) and Reunion (Channell et al., 2003) Subchrons was used to construct age models.

The magnetic susceptibility of whole-core sections was measured on two separate track systems. Whole-core sections were measured on a Fast Track system used to rapidly acquire magnetic susceptibility data for stratigraphic correlation (see **"Composite section"**). After whole cores warmed to room temperature, magnetic susceptibility measurements were made as part of the MST analyses (see **"Physical properties"**).

# Composite section

Paleomagnetic and paleoclimatic objectives of Expedition 303 necessitated the recovery of complete stratigraphic sections, yet stratigraphers have demonstrated that a continuous section is rarely recovered from a single ODP or IODP borehole because of core-recovery gaps between successive APC and extended core barrel cores, despite 100% or more nominal recovery (Ruddiman et al., 1987; Hagelberg et al., 1995). Construction of a complete section, referred to as a composite splice, requires combining stratigraphic intervals from two or more holes cored at the same site. To maximize the probability of bridging core-recovery gaps in successive holes, the depths below the seafloor from which cores are recovered are offset between the holes. This practice ensures that most intercore intervals missing within a given hole are recovered in at least one of the adjacent holes. During Expedition 303, three or more holes were cored at all but one site and used to construct composite sections.

Our composite sections and splice construction methodology follows one that has been successfully employed during a number of previous ODP legs (e.g., Hagelberg et al., 1992; Curry, Shackleton, Richter, et al., 1995; Jansen, Raymo, Blum, et al., 1996; Lyle, Koizumi, Richter, et al., 1997; Gersonde, Hodell, Blum, et al., 1999, Wang, Prell, Blum, et al., 2000; Mix, Tiedemann, Blum, et al., 2003; Zachos, Kroon, Blum, et al., 2004; among others). The assem-

bly and verification of a complete composite stratigraphic section requires the construction of a composite depth scale. Other depth scales (discussed in **"Compositing,"** below) can be implemented using logging data and/or combining splicing and driller depths.

Construction of a continuous spliced section is a two-step process involving compositing and splicing.

## Compositing

Cores from the various holes must first be composited, which entails stratigraphically correlating and depth shifting cores relative to each other. Such correlation enables development of a composite depth scale referred to as meters composite depth. The mcd scale differs from the traditional (hole specific) depth scale, called the meters below seafloor scale. Mbsf is based on the length the drill string is advanced on a core-by-core basis and is often inaccurate because of ship heave (which is not compensated for in APC coring), tidal variations in sea level, and other sources of error. In contrast, the mcd scale is built by assuming that the uppermost sediment (commonly referred to as the mudline) in the first core from a given hole is the sediment/water interface. This core becomes the "anchor" in the composite depth scale and is typically the only one in which depths are the same on both the mbsf and mcd scales. From this anchor, core logging data are correlated among holes downsection. For each core, a depth offset (a constant) that best aligns the observed lithologic variations to the equivalent cores in adjacent holes is added to the mbsf depth in sequence down the holes. Depth offsets are often chosen to optimize correlation of specific features that define splice levels in cores from adjacent holes.

For Expedition 303, the mcd scale and the splice are based on the stratigraphic correlation of data from the IODP whole-core Fast Track, the MST, and the AMST. Core-logging data were collected at 2.5, 5, or 6 cm intervals. We used magnetic susceptibility (the data are referred to as MSCL if collected using the Fast Track or MS-MST if collected using the MST), gamma ray attenuation (GRA) bulk density, natural gamma radiation (NGR), and reflectance (L\*, a\*, and b\*). All of these measurements are described in **"Physical properties."**

The raw stratigraphic data were imported into the shipboard Splicer software program (version 2.2) and culled as necessary to avoid incorporating anomalous data influenced by edge effects at section boundaries. Splicer was used to assess the strati-

graphic continuity of the recovered sedimentary sequences at each drill site and to construct the mcd scale and splice.

Because depth intervals within cores are not squeezed or stretched by Splicer, not all correlative features can be aligned. Stretching or squeezing between cores from different holes may reflect small-scale differences in sedimentation and/or distortion caused by the coring and archiving processes. The tops of APC cores are generally stretched and the bottoms compressed, although this is lithology dependent. In addition, sediment (especially unconsolidated mud, ash, sand, and gravel) occasionally falls from higher levels in the borehole onto the tops of cores as they are recovered, and, as a result, the top 20–100 cm of many cores is not reliable.

Correlations among cores from adjacent holes are evaluated visually and statistically (by cross-correlation within a 2 m depth interval). Depth-shifted data are denoted by mcd. Each site chapter includes a table that summarizes the depth offsets for each core. These tables are necessary for converting mbsf to mcd scales. The mcd for any point within a core equals the mbsf plus the cumulative offset. Correlation at finer resolution is not possible with Splicer because depth adjustments are applied linearly to individual cores; no adjustments, such as squeezing and stretching, are made within cores. Such fine-scale adjustment is possible postcruise (e.g., Hagelberg et al., 1995).

## Splicing

Once all cores have been depth-shifted and stratigraphically aligned, a composite section is built by splicing segments together from multiple holes to form a complete record at a site. It is composed of core sections from adjacent holes so that coring gaps in one hole are filled with core intervals from an adjacent hole. The splice does not contain coring gaps, and an effort has been made to minimize inclusion of disturbed sections. The shipboard splice is ideally suited to guide core sampling for detailed paleoceanographic studies. Each site chapter includes a table and a figure that summarize the intervals from each hole used to construct the splice. Additional splices may be constructed postcruise as needed.

The choice of tie points (and hence of a splice) is a somewhat subjective exercise. Our method in the construction of a splice followed three rules:

1. Where possible, avoid using the top and bottom 1 m of cores, where disturbance resulting from drilling artifacts (even if not apparent in core logging data) is most likely;

2. Attempt to incorporate those portions of the recovered core that are most representative of the overall stratigraphic section of the site; and

3. Try to minimize tie points to simplify sampling.

The length of the spliced section (on the mcd scale) at a given site is typically ~5%–15% greater than the length of the cored section in any one hole, as indicated by the mbsf scale. This expansion is commonly attributed to sediment expansion resulting from elastic rebound, stretching during the coring process, gas expansion during the core recovery process, and other factors (e.g., Moran, 1997).

Ideally, the base of the mcd scale is the bottom of the deepest core recovered from the deepest hole. In practice, however, the base often occurs where core recovery gaps align across all holes or the data quality does not allow reliable correlations between holes. Cores below this interval cannot be directly tied into the overlying and continuous mcd. However, below the base of the continuous mcd, cores from two or more holes can sometimes be correlated with each other to create a floating splice. In this case, an mcd was assigned to the section below the splice by adding the greatest cumulative offset to the first core below the splice and beginning the floating splice from that point in the section.

## Corrected meters composite depth

We also provide corrected meters composite depth (cmcd) in our depth conversion tables. This scale is intended to correct the mcd scale for empirically observed core expansion. A growth factor (GF) is calculated by fitting a line to mbsf versus mcd. A cmcd datum is produced by dividing mcd by GF over a sufficiently long interval so that random variations in drill pipe advance due to ship heave, tides, and other factors are negligible. This operation produces a complete stratigraphic sequence that is the same length as the total depth cored. The cmcd scale is a close approximation of the actual drilling depth scale.

## Fast Track

The Oregon State University Fast Track for measuring magnetic susceptibility on cores as soon as possible following recovery was first introduced during ODP Leg 202. During Expedition 303, we tested the first deployment of the IODP MSCL Fast Track system, which uses two magnetic susceptibility loops on a single track to speed up analysis time. This setup was not satisfactory (see **"Physical properties"**) and we quickly converted the Fast Track to a single sensor

measuring at 6 cm intervals beginning with Hole 1302B. This helped us to make drilling adjustments aimed at ensuring the recovery of a complete stratigraphic section while allowing us to run the MST at a slower rate to optimize data quality (longer measurement time yielding greater analytic precision and, in many cases, higher spatial resolution) because we did not need its data to assess recovery of a complete section at most sites.

## Depths in splice tables versus Janus depths

The depth of a core interval recorded for a tie point in a splice table is not always the same as the depth for the same core interval returned by most database queries. This is because the tie point depth is based on the liner length, which is measured when the cores are cut into sections on the catwalk. The cores are analyzed on the MST almost immediately after this liner-length measurement. At some later time, typically 10–36 h after being analyzed by the MST, core sections are split and analyzed further (see **"Core handling and analysis"** in "Introduction"). At this time, the section lengths are measured again and are archived as "curated lengths." General database queries return depths based on the curated liner lengths. Because the sections are usually expanding during the period between the two measurements, the curated length is almost always longer than the initial liner length. Thus, the depths associated with the MST data used to construct the splice table are not identical to the final depths the database assigns to a given interval. This leads to small differences (usually between 0 and 5 cm) between the mbsf and mcd recorded in a splice table and the depths reported in other places for the same core interval. We have chosen not to change these depths to be compatible with Janus because this would not improve their accuracy. For consistency, we recommend that all postcruise depth models use or build on mcd values provided in the Janus database.

# Geochemistry

The shipboard geochemistry program for Expedition 303 included characterization of (1) volatile hydrocarbons and other gases, (2) interstitial water, and (3) sedimentary inorganic and organic carbon, nitrogen, and sulfur. These analyses were carried out as part of the routine shipboard safety and pollution prevention requirements and to provide the standard shipboard data set and preliminary information for shore-based research.

## Sediment gas sampling and analysis

During Expedition 303, the compositions and concentrations of volatile hydrocarbons in the sediments were monitored once per core. Gas samples were obtained by two different methods. First, the routine headspace procedure (Pimmel and Claypool, 2001) involved placing ~5 cm³ of sediment sample in a 21.5 cm³ glass serum vial that was sealed with a septum and metal crimp cap immediately after core retrieval on deck. In the shipboard laboratory, the glass vial was heated at 60°C for 30 min. A 5 cm³ volume of gas from the headspace in the vial was removed with a glass syringe for analysis by gas chromatography. A second gas sampling procedure was used for gas pockets or expansion voids that appeared in the core while it was still in the core liner. A device with a heavy-duty needle was used to penetrate the core liner, and an attached syringe was employed to collect the gas. Thus method was applied only once during Expedition 303 on Sample 303-U1304A-14H-2, 50–51 cm.

Headspace and gas samples were both analyzed using a Hewlett-Packard 6890 Plus gas chromatograph (GC) equipped with a 2.4 m × 3.2 mm stainless steel column packed with 80/100 mesh HayeSep-S and a flame ionization detector (FID). This analytical system quickly measures the concentrations of methane ($C_1$), ethane ($C_2$), ethene ($C_{2=}$), propane ($C_3$), and propene ($C_{3=}$). The gas syringe was directly connected to the GC via a 1 cm³ sample loop. Helium was used as the carrier gas, and the GC oven temperature was held at 90°C. Data were collected and evaluated with the Hewlett-Packard 3365 Chemstation data-handling program. Calibrations were conducted using analyzed gases, and gas concentrations were measured in parts per million by volume.

A natural gas analyzer (NGA) was used to measure concentrations of hydrocarbons through $C_6$ and nonhydrocarbon gases on void gas Sample 303-U1304A-14H-2, 50–51 cm. The NGA system consists of a Hewlett-Packard 6890 Plus GC equipped with multiport valves that access two different column and detector combinations. Hydrocarbons from methane to hexane were measured with a 60 m × 0.32 mm DB-1 capillary column and an FID. The GC oven holding this column was heated from 80° to 100°C at 8°C/min and then to 200°C at 30°C/min. Nonhydrocarbon gases were isothermally analyzed at the same time using a sequence of packed columns (15 cm HayeSep-R column connected to a 1 m molecular sieve column and a 2 m Poropak-T column) and thermal conductivity detectors (TCDs). Helium was the carrier gas in both systems, and Hewlett-Packard Chemstation was used for data acquisition and processing. Chromatographic response was calibrated against preanalyzed standards. Gas contents are reported in ppmv.

## Interstitial water sampling and chemistry

Interstitial waters were extracted from 5 cm long whole-round sediment sections that were cut and capped immediately after core retrieval on deck. At each site, samples were taken from each core for the upper 60 m and at intervals of every third core thereafter to total depth. In addition to whole-round samples, small plug sediment samples of ~10 cm³ were taken with a syringe at two per core for the upper 60 m and at one per core for 60–100 mbsf for shore-based analyses of oxygen isotopes, deuterium, and chlorinity at high precision. The small plug samples were taken from the working half at the time of sectioning on deck. This sampling technique was used to obtain high-resolution interstitial water samples while maintaining the integrity of the composite section.

In the shipboard laboratory, whole-round sediment samples were removed from the core liner, and the outside surfaces of the sediment samples were carefully scraped off with spatulas to minimize potential contamination with drill fluids. Sediment samples were then placed into a Manheim titanium squeezer and squeezed at ambient temperature with a Carver hydraulic press (Manheim and Sayles, 1974). Interstitial water samples discharged from the squeezer were passed through 0.45 µm polyethersulfone membrane filters, collected in plastic syringes, and stored in plastic sample tubes for shipboard analyses or archived in glass ampoules and/or heat-sealed acid-washed plastic tubes for shore-based analysis.

Shipboard analyses of whole-round interstitial water samples followed the procedures outlined by Gieskes et al. (1991) and Murray et al. (2000) with modifications as summarized below. Salinity was measured with an Index Instruments digital refractometer. Alkalinity and pH were measured by Gran titration with a Brinkman pH electrode and a Metrohm 702 SM autotitrator. $NH_4^+$ concentrations were analyzed by spectrophotometric methods with a Milton Roy Spectronic 301 spectrophotometer. For the analyses of $Mn^{2+}$, $Fe^{2+}$, B, $Sr^{2+}$, $Ba^{2+}$, $Li^+$, and $H_4SiO_4$ concentrations, a Jobin Yvon JY2000 inductively coupled plasma–atomic emission spectrometer (ICP-AES) was used. Concentrations of $SO_4^{2-}$, $Mg^{2+}$, $Ca^{2+}$, and $K^+$ were determined with a Dionex DX-120 ion chromatograph. $Cl^-$ was measured by silver nitrate titration method using a Metrohm 665 titrator. $Na^+$ values reported in site reports were determined by charge balance calculations using the following equation:

$$Na^+ = 2SO_4^{2-} + Cl^- + Alk - K^+ - 2Mg^{2+} - 2Ca^{2+},$$

where Alk is alkalinity. Ion charges of minor dissolved species are neglected in this calculation. Chemical data for interstitial water are reported in molar concentration units.

Analytical precision for each of the techniques was monitored through multiple analyses of International Association of Physical Sciences Organization (IAPSO) standard seawater solution or other standard solutions. For calibration of the ion chromatographic method, IAPSO solutions, diluted with 18 MΩ deionized water to 0%, 10%, 20%, 40%, 60%, 80%, and 100%, were used at the beginning of each batch (i.e., site) run. Elemental analysis by ICP-AES was modified from Murray et al. (2000) as outlined in Shipboard Scientific Party (2003). Specifically, a "master standard" was prepared by blending standard solutions of $Mn^{2+}$, $Fe^{2+}$, B, $Sr^{2+}$, $Ba^{2+}$, and $Li^+$ and a silicon reference solution (sodium silicate) in an acidified (1.25% $HNO_3$, by volume) sodium chloride matrix (17.5 g NaCl/L) diluted with 18 MΩ deionized water. This solution was diluted to 0%, 3%, 5%, 10%, 30%, 50%, and 100% with a NaCl/$HNO_3$ matrix (35 g NaCl + 2.5% $HNO_3$/1 L) to generate "working standard" solutions. Calibrations were made for each of the chemical constituents measured by ICP-AES using the working standard solutions diluted with a matrix solution (2.5% $HNO_3$ + 10 ppm yttrium as an internal standard) prior to each batch run. The precision of the ICP-AES measurements was assessed by multiple analyses of the IAPSO standard and a "drift solution," which was made by diluting the master standard with NaCl/$HNO_3$ matrix and 18 MΩ deionized water. Analytical precision for the measured constituents in the interstitial water is reported in Table **T2.**

### Sedimentary inorganic and organic carbon, nitrogen, and sulfur concentrations

Inorganic carbon concentrations were determined using a Coulometrics 5011 carbon dioxide coulometer equipped with a System 140 carbonate analyzer at a frequency of two per core. Samples of ~10 mg of freeze-dried, ground sediment were reacted with 2N HCl. The liberated $CO_2$ was backtitrated to a colorimetric end point. Calcium carbonate content (in weight percent) was calculated from the inorganic carbon (IC) content with the assumption that all inorganic carbon is present as calcium carbonate:

$$CaCO_3 \text{ (wt\%)} = IC \text{ (wt\%)} \times 8.33.$$

No corrections were made for other carbonate minerals. The coulometer was calibrated with pure $CaCO_3$ powder during the expedition, and the analytical precision (expressed as 1σ standard deviation

of the mean of multiple determinations of a standard) for weight percent IC was ±1.3% (for Sites U1302–U1307).

Total carbon (TC), total nitrogen (TN), and total sulfur were determined using a Carlo Erba 1500 CNS analyzer on a subset of the samples used for inorganic carbon determinations. Aliquots of 10 mg of freeze-dried, ground sediment with ~10 mg $V_2O_5$ oxidant were combusted at 1000°C in a stream of oxygen. Nitrogen oxide was reduced to $N_2$, and the mixture of $N_2$, $CO_2$, $H_2O$, and $SO_2$ gases was separated by a GC and detection performed by a TCD. All measurements were calibrated by comparison to pure sulfanilamide as standard. Analytical precision for TC and TN was 4.4% and 6.7%, respectively (for Sites U1302–U1307). Contents of total organic carbon (TOC) (in weight percent) were calculated as the difference between total carbon and inorganic carbon:

$$TOC \text{ (wt\%)} = TC \text{ (wt\%)} - IC \text{ (wt\%)}.$$

The carbon/nitrogen atomic ratios of organic materials were calculated from TOC and total nitrogen concentrations to identify sources of organic matter (i.e., marine or terrestrial). No pyrolysis analyses were performed during Expedition 303.

# Physical properties

Physical properties were measured on core material recovered during Expedition 303 to

- Allow real-time stratigraphic correlation and feedback to the drillers;
- Provide further data for the hole-to-hole core correlation of any given site and for the construction of composite stratigraphic sequences;
- Detect changes in sediment properties that could be related to lithologic changes, diagenetic features, or consolidation history;
- Provide the dry density records needed for computing mass accumulation rates;
- Identify natural and/or coring-induced discontinuities; and
- Provide data to aid interpretation of seismic reflection and downhole geophysical logs.

Magnetic susceptibility, GRA bulk density, compressional wave velocity ($V_P$), and NGR were measured on the whole-core MST. Magnetic susceptibility was also measured with the MSCL on whole-round core sections immediately after recovery. These measurements aided real-time stratigraphic correlation without being limited by the time constraints of MST measurements.

Thermal conductivity was also measured on whole-round cores. Split-core measurements on the work-

ing half of the core included $V_p$, with the IODP *P*-wave sensor number 3 (PWS3—measuring perpendicular to the core axis), and moisture and density (MAD). A comprehensive description of most of the methodologies and calculations used in the *JOIDES Resolution* physical properties laboratory can be found in Blum (1997).

## Magnetic susceptibility core logger sampling strategy

Rapid stratigraphic correlation of cores from adjacent holes and real-time feedback to drillers for recovering complete stratigraphic sections at all sites was a major cruise objective. The MSCL, an automated dedicated Fast Track for rapid measurement of magnetic susceptibility, was used to provide a nondestructive proxy of sediment variability to the stratigraphic correlators without delay. Measurements were made prior to warming as soon as whole-core sections became available. The MSCL system employs a Geotek tracking system with dual Bartington MS2C meters and two 80 mm internal diameter coils separated by 45 cm. Because of the proximity of the coils, different frequencies were used to reduce interference, 0.621 kHz for the first and 0.513 kHz for the second. Distinct correction factors (1.099 and 0.908, respectively) must be used to synchronize data acquired from the two loops. Measurements were taken every 10 cm. The use of two loops allowed simultaneous interlaced measurements, decreasing the sampling interval to 5 cm. The dual loop system, however, introduced noise into the data because the two loops were not precisely cross-calibrated and had independent drift characteristics. The MSCL was converted to a single loop measuring at 6 cm intervals after Hole 1302A. The Geotek core pusher system measures sections continuously thereby minimizing edge effects at section breaks. Cores were measured prior to warming to room temperature, and drift corrections were not applied.

The MST susceptibility meter (a Bartington MS2C meter with an 80 mm coil diameter driven at 0.565 kHz frequency) was set on SI units, and the output values were stored in the database. The width at half-height of the response function of the susceptibility coil is ~4 cm, according to Blum (1997), and the sensing region corresponds to a cored volume of 160 cm$^3$. To convert the stored values to SI units of volume susceptibility, they should be multiplied by 10$^{-5}$ and by a correction factor to take into account the volume of material within the response function of the susceptibility coils. For a standard IODP core, this factor is ~6.8 (Thomas et al., 2003), based on laboratory/ship comparisons for Leg 162 sediments.

## Archive multisensor track sampling strategy

Two instruments were mounted on the AMST: the Minolta spectrophotometer measuring diffuse color reflectance and a point magnetic susceptibility meter, which was not used during this cruise. Color reflectance was measured at 2.5 cm throughout Expedition 303 cores (for color reflectance see **"Spectrophotometry [color reflectance]"** in "Lithostratigraphy").

## Multisensor track sampling strategy

Magnetic susceptibility and GRA bulk density were measured nondestructively with the MST on all whole-round core sections. Compressional wave velocity was measured on some core sections from Site U1302A, until the equipment broke down. To optimize MST performance, sampling intervals and measurement residence times were the same for all sensors for any one core. Sampling intervals were therefore set at 2.5 or 5 cm, depending on time constraints, with most cores measured at 2.5 cm intervals. These sampling intervals are common denominators of the distances between the sensors installed on the MST (30–50 cm) and allow truly simultaneous measurements and therefore optimal use of total measurement times.

We endeavored to set core logging times to achieve the best possible depth resolution. Longer measurement residence times were selected if required to improve measurement precision. Residence times varied from 3 to 5 s, with most cores measured at 5 s per sample.

The total time availability for MST logging at a site was predicted based on the operational time estimate for the site, subsequent transit time, and any other time available before core was on deck at the subsequent site. Sampling spacing and residence times were then optimized to use the total available time (e.g., 2.5 cm and 5 s [~2 h/core]; 5 cm and 5 s [~1.2 h/core]; 5 cm and 3 s [fast logging, ~0.9 h/core]).

## Magnetic susceptibility

Magnetic susceptibility is a measure of the degree to which a material can be magnetized by an external magnetic field. It provides information on the magnetic composition of the sediments that often can be related to mineralogical composition (e.g., terrigenous versus biogenic materials) and/or diagenetic overprinting. Magnetite and a few other iron oxides with ferromagnetic (s.l.) characteristics have a specific magnetic susceptibility several orders of magnitude higher than clay, which has paramagnetic prop-

erties. Carbonate, silica, water, and plastics (core liner) have small negative values of magnetic susceptibility. Sediments rich in biogenic carbonate and opal therefore have generally low magnetic susceptibility, even negative values, if practically no clay or magnetite is present. In such cases, measured values approach the detection limit of magnetic susceptibility meters.

Magnetic susceptibility was measured with the Bartington Instruments MS2C system on both the MST and MSCL. The output of the magnetic susceptibility sensors can be set to centimeter-gram-second (cgs) units or SI units. The IODP standard is the SI setting. However, to actually obtain the dimensionless SI volume-specific magnetic susceptibility values, the instrument units stored in the IODP database must be multiplied by a correction factor to compensate for instrument scaling and the geometric ratio between core and loop dimensions, as described above.

A common operational problem with the Bartington meter is that the 1 s (residence time) measurements are rapid but not precise enough for biogenic-rich sediments, and the 10 s measurements are much more precise but take a prohibitively long time to measure at the desired sampling interval of 2.5–5 cm. The MST program was therefore equipped with the option to average any number of 1 s measurements, and we usually averaged five such measurements.

## Gamma ray attenuation bulk density

Bulk density reflects the combined effect of variations in porosity, grain density (dominant mineralogy), and coring disturbance. Porosity is mainly controlled by lithology and texture (e.g., clay, biogenic silica, and carbonate content, and grain size and sorting), compaction, and cementation.

The GRA densitometer uses a 10 mCi $^{137}$Cs capsule as the gamma ray source, with the principal energy peak at 0.662 MeV, and a scintillation detector. The narrow collimated peak is attenuated as it passes through the center of the core. Incident photons are scattered by the electrons of the sediment material by Compton scattering.

The attenuation of the incident intensity ($I_0$) is directly related to the electron density in the sediment core of diameter ($D$), which can be related to bulk density given the average attenuation coefficient (in micrometers) of the sediment (Evans, 1965; Harms and Choquette, 1965). Because the attenuation coefficient is similar for most common minerals and aluminum, bulk density is obtained through direct calibration of the densitometer using aluminum rods of different diameters mounted in a core liner that is filled with distilled water. The GRA densitometer has a spatial resolution of <1 cm.

## Natural gamma radiation

Terrigenous sediment is often characterized by NGR from K, Th, and U, which are present mostly in clays but can also originate from heavy minerals or lithic grains. Uranium often dominates the NGR in carbonate-rich sediments with little terrigenous input. Uranium concentration is largely controlled by organic matter flux to the seafloor and the existing redox conditions there. It is also mobile and can migrate to certain layers and diagenetic horizons.

The natural gamma ray system consists of four shielded scintillation counters with 3 inch × 3 inch doped sodium iodide crystals, arranged at 90° from each other in a plane orthogonal to the core track. The NGR response curve is ~17 cm (full-width half maximum), an interval that could be considered a reasonable sampling interval. Measurement precision is a direct function (inverse of square root) of the total counts ($N$) accumulated for one measurement, according to Poisson's law of random counting error. $N$ is the product of the intrinsic activity of the material measured and the total measurement time. Therefore, one seeks to maximize the measurement time to improve data quality. Unfortunately, time constraints on core logging during the cruise do not permit long counting times. Furthermore, NGR is measured every 2.5 or 5 cm (same sampling interval as other MST measurements for optimal MST efficiency) and, therefore, only for a relatively short time (typically 5 s). It may be necessary, particularly in low-activity material, to integrate (or smooth) several adjacent measurements to reduce the counting error to an acceptable level. Five-point smoothing is a reasonable data reduction in view of the relatively wide response curve of the sensors (see Blum, 1997, for more detailed discussions).

## Thermal conductivity

Thermal conductivity was measured on one section of unsplit soft-sediment core from each Hole A (usually at 75 cm) at Sites U1302–U1304. Heat flow measurements were discontinued after one of the two remaining downhole APC temperature (APCT) tools was damaged at Site U1302 on downhole debris or large dropstones. Because heat flow determinations were not critical to the cruise objectives, APCT deployment was discontinued to conserve existing tools. Thermal conductivity measurements were discontinued after cancellation of APCT runs. The thermal conductivity estimates along with downhole temperature tool measurements at Site U1302 were used for the estimation of heat flow. This physical

property is dependent on the material's chemical composition, density, and porosity.

We used the Teka TK04 measurement system, which employs the transient linear heat source method with a needle probe that is inserted into the soft sediment. The TK04 uses an automated routine to find the conductivity by least-squares fitting to the measured temperature time series. No calibration was required for this system, since each probe is calibrated prior to leaving the factory. Measurements were taken on the whole-core sections after their temperature was equilibrated to laboratory temperature. Special care was taken to minimize measurement drift by covering the needle point of entry and insulating it from external temperature shifts.

### *P*-wave velocity

*P*-wave velocity in marine sediments varies with lithology, porosity and bulk density, state of stress (such as lithostatic pressure), fabric or degree of fracturing, degree of consolidation and lithification, occurrence and abundance of free gas and gas hydrate, and other properties. *P*-wave velocity was measured with two systems during Expedition 303: with the MST-mounted *P*-wave logger (PWL) on whole-round cores (Schultheiss and McPhail, 1989) and with the PWS3 on every section of the split cores. All IODP *P*-wave piezoelectric transducers transmit a 500 kHz compressional wave pulse through the core at a repetition rate of 1 kHz.

Traveltime is determined by the software, which automatically picks the arrival of the first wavelet to a precision of 50 ns. It is a challenge for an automated routine to pick the first arrival of a potentially weak signal with significant background noise. The search method skips the first positive amplitude and finds the second positive amplitude using a detection threshold limit, typically set to 30% of the maximum amplitude of the signal. Then it finds the preceding zero crossing and subtracts one period to determine the first arrival. To avoid extremely weak signals, minimum signal strength can be set (typically to 0.02 V) and weaker signals ignored. To avoid cross-talk signals at the beginning of the record from the receiver, a delay (typically set to 0.01 ms) can be set to force the amplitude search to begin in the quiet interval preceding the first arrival. In addition, a trigger (typically 4 V) is selected to initiate the arrival search process, and the number of waveforms to be stacked (typically 5) can also be set. Linear voltage differential transducers determine length of the travel path.

The *P*-wave velocity systems require two types of calibration, one for the displacement of the transducers and one for the time offset. For the displacement cal-

ibration, five acrylic standards of different thickness are measured and the linear voltage-distance relationship determined using least-squares analyses. For the time offset calibration, room-temperature water in a plastic bag is measured multiple times with different transducer displacements. The inverse of the regression slope is equal to the velocity of sound in water, and the intercept represents the delay in the transducers.

During Expedition 303 we observed a discrepancy between the PWL and PWS3 measurements. Troubleshooting was performed, but the exact cause of the problem could not be found. The offset between PWL and PWS3 is 2%–3% in most cases. This is a long-standing problem not unique to Expedition 303.

### Moisture content and density

Samples of 10 $cm^3$ were taken from the working-half sections with a piston minicorer and transferred into previously calibrated 10 mL glass vials. Usually one sample from the base of Section 1 and one sample from the top of Section 6 were taken. To minimize the destruction of the available sediment in the specific sampling zones, a further 2 $cm^3$ was collected for carbonate analysis as close as possible to the MAD sample.

Wet and dry weights were determined with twin Scientech 202 electronic balances, which allow for effect of ship's motion on the balance and give a precision better than 1%.

The samples were dried in a convection oven at a temperature of 105° ± 5°C for a period of 24 h. Dry volume was measured in a helium-displacement penta-pycnometer with an uncertainty of 0.02 $cm^3$. This equipment allowed the simultaneous analysis of four different samples and a calibration sphere and took around 15–20 min. Three measurements were averaged per sample. The calibration sphere was cycled from cell to cell of the pycnometer during each batch, so that all cells could be checked for accuracy at least once every five runs.

# Downhole measurements

Downhole logs provide continuous in situ geophysical parameters within a borehole. These measurements are used to assess the physical, chemical, and structural characteristics of formations penetrated by drilling and thus provide a means of reconstructing the stratigraphy, lithology, and mineralogy of a sequence. Well logging is typically undertaken in the deepest hole drilled at any one site. Where core recovery is poor or disturbed, downhole logs are often

the most reliable source of information; where core recovery is good, core data can be correlated with logging data to refine stratigraphy and unit characterization. Downhole logging operations begin after the hole has been cored and flushed with a viscous drilling fluid. The drilling assembly is then pulled up to ~70 mbsf, and the logging tools are passed through the drill pipe into the open hole. The logging tools are joined together into tool strings so that compatible tools are run together. Each tool string is lowered separately to the base of the hole and measurement takes place as the tool string is raised at a constant rate between 275 and 500 m/h (see "Downhole Measurements" in the individual site chapters). A wireline heave compensator is used to minimize the effect of the ship's heave on the tool position in the borehole (Goldberg, 1990). Further information on the procedures and wireline tools used during Expedition 303 can be found at **www.ldeo.columbia.edu/TOOLS_TECH/index.html.**

## Logging tools and tool strings

During Expedition 303, the following logging tool strings were available for deployment (Fig. **F8;** Table **T3**) (see the **"Site U1305"** chapter for actual logging runs):

- The triple combination ("triple combo") string, which consists of the Hostile Environment Gamma Ray Sonde (HNGS), Accelerator Porosity Sonde (APS), the Hostile Environment Litho-Density Sonde (HLDS), the Dual Induction Tool model E (DIT-E), and two Lamont-Doherty Earth Observatory (LDEO) tools, the Multi-Sensor Spectral Gamma Ray Tool (MGT), and the Temperature/Acceleration/Pressure (TAP) tool; and

- The FMS-sonic tool string, which consists of the Scintillation Gamma Ray Tool (SGT), the Dipole Sonic Imager (DSI), the General Purpose Inclinometer Tool (GPIT), and the Formation Micro-Scanner (FMS).

## Principles and uses of the logging tools

The properties measured by each tool, sampling intervals, and vertical resolutions are summarized in Table **T3.** Explanations of tool name acronyms and their measurement units are summarized in Table **T4.** More detailed descriptions of individual logging tools and their geological applications can be found in Ellis (1987), Goldberg (1997), Rider (1996), Schlumberger (1989, 1994), Serra (1984, 1986, 1989), and the LDEO Borehole Research Group (BRG) Wireline Logging Services Guide (Lamont-Doherty Earth Observatory-Borehole Research Group, 2001).

## Natural radioactivity

Three wireline spectral gamma ray tools were used during Expedition 303 to measure and classify natural radioactivity in the formation: the HNGS, the SGT, and the MGT. The HNGS measures the natural gamma radiation from isotopes of K, Th, and U and uses a five-window spectroscopic analysis to determine concentrations of radioactive $^{40}K$ (in wt%), $^{232}Th$ (in ppmv), and $^{238}U$ (in ppmv). The HNGS uses two bismuth germanate scintillation detectors for gamma ray detection with full spectral processing. The spectral analysis filters out gamma ray energies below 500 keV, eliminating sensitivity to bentonite or potassium chloride (KCl) in the drilling mud and improving measurement accuracy. The HNGS also provides a measure of the total standard gamma ray emission and uranium-free or computed gamma ray emission measured in American Petroleum Institute gamma ray units. The HNGS response is influenced by the borehole diameter and the weight and concentration of bentonite or KCl present in the drilling mud. KCl may be added to the drilling mud to prevent freshwater clays from swelling and forming obstructions. All of these effects are corrected during processing of HNGS data at LDEO-BRG.

The SGT uses a sodium iodide scintillation detector to measure the total natural gamma ray emission, combining the spectral contributions of $^{40}K$, $^{238}U$, and $^{232}Th$ concentrations in the formation. The SGT is not a spectral tool but provides high-resolution total gamma ray data for depth correlation between logging strings. It is included in the FMS-sonic tool string to provide a reference log to correlate depth between different logging runs. In the FMS-sonic tool string, the SGT is placed between the HNGS and the MGT, providing correlation data to a deeper level in the hole.

The MGT was developed by LDEO-BRG to improve the vertical resolution of natural gamma ray logs by using an array of four short detector modules with 60 cm spacing. Each module comprises a small 2 inch × 4 inch NaI detector, a programmable 256-channel amplitude analyzer, and a 241 Am calibration source. The spectral data are subsequently recalculated to determine the concentration of K, Th, and U radioisotopes or their equivalents. The spectral data from individual modules are sampled four times per second and stacked in real time based on the logging speed. This approach increases vertical resolution by a factor of two to three over conventional tools, while preserving comparable counting efficiency and spectral resolution. The radius of investigation depends on several factors: hole size, mud density, formation bulk density (denser formations display a slightly lower radioactivity), and the energy

of the gamma rays (a higher energy gamma ray can reach the detector from deeper in the formation). The MGT also includes an accelerometer channel to improve data stacking by the precise measurement of logging speed. Postcruise corrections for borehole size and tool sticking are possible, based, respectively, on the caliper and acceleration data.

## Density

Formation density was determined with the HLDS. The tool contains a radioactive cesium ($^{137}Cs$) gamma ray source (622 keV) and far and near gamma ray detectors mounted on a shielded skid, which is pressed against the borehole wall by a hydraulically activated eccentralizing arm. Gamma rays emitted by the source experience both Compton scattering and photoelectric absorption. Compton scattering involves the ricochet of gamma rays off electrons in the formation via elastic collision, transferring energy to the electron in the process. The number of scattered gamma rays that reach the detectors is directly related to the number of electrons in the formation, which is related to bulk density. Porosity may also be derived from this bulk density if the matrix density is known.

The HLDS also measures the photoelectric effect factor (PEF) caused by absorption of low-energy gamma rays. Photoelectric absorption occurs when gamma rays reach <150 keV after being repeatedly scattered by electrons in the formation. As the PEF depends on the atomic number of the elements in the formation, it is essentially independent of porosity. Thus, the PEF varies according to the chemical composition of the formation. The PEF values can be used in combination with HNGS curves to identify different types of clay minerals. Coupling between the tool and borehole wall is essential for good HLDS logs. Poor contact results in underestimation of density values. Both density correction and caliper measurement of the hole are used to check the contact quality.

## Porosity

Formation porosity was measured with the APS. The sonde incorporates a minitron neutron generator that produces fast neutrons (14.4 MeV) and five neutron detectors (four epithermal and one thermal) positioned at differing intervals from the minitron. The measurement principle involves counting neutrons that arrive at the detectors after being slowed by neutron absorbers surrounding the tool. The highest energy loss occurs when neutrons collide with hydrogen nuclei, which have practically the same mass as the neutron (the neutrons simply bounce off heavier elements without losing much energy). If hydrogen concentration is low, as in low-porosity

formations, neutrons can travel farther before being captured, and the count rates increase at the detector. The opposite effect occurs when the water content is high. However, because hydrogen bound in minerals such as clays or in hydrocarbons also contributes to the measurement, the raw porosity value is often an overestimate. Upon reaching thermal energies (0.025 eV), the neutrons are captured by the nuclei of Cl, B, Cd, and other rare earth and trace elements with large capture cross sections, resulting in a gamma ray emission. This neutron capture cross section ($\Sigma f$) is also measured by the tool.

## Electrical resistivity

The DIT-E was used to measure electrical resistivity. The DIT-E provides three measures of electrical resistivity, each with a different depth of penetration. The two induction devices (deep and medium depths of penetration) transmit high-frequency alternating currents through transmitter coils, creating magnetic fields that induce secondary currents in the formation. These currents produce a new inductive signal, proportional to the conductivity of the formation, which is measured by the receiving coils. The measured conductivities are then converted to resistivity (measured in ohm-meters). For the shallow penetration resistivity, the current necessary to maintain a constant voltage drop across a fixed interval is measured; it is a direct measurement of resistivity. Sand grains and hydrocarbons are electrical insulators, whereas ionic solutions and clays are more conductive. Electrical resistivity can therefore be used to evaluate porosity (via Archie's law) if fluid salinity is known.

## Temperature, acceleration, and pressure

Downhole temperature, acceleration, and pressure were measured with the LDEO high-resolution TAP tool run in memory mode. The tool uses fast- and slow-response thermistors to detect borehole fluid temperature at two different rates. The fast-response thermistor detects small, abrupt changes in temperature, whereas the slow-response thermistor more accurately estimates temperature gradients and thermal regimes. A pressure transducer is used to activate the tool at a specified depth, typically 200 m above seafloor. A three-axis accelerometer measures tool movement downhole, providing data for analyzing the effects of heave on a deployed tool string. The acceleration log can aid in deconvolving heave effects postcruise. The elapsed time between the end of drilling and the logging operation is generally not sufficient to allow the borehole to reach thermal equilibrium following circulation of the drilling fluid. Nevertheless, it is possible to identify abrupt

temperature changes that may represent localized fluid flow into the borehole, indicative of fluid pathways and fracturing and/or breaks in the temperature gradient that may correspond to contrasts in permeability at lithologic boundaries.

## Acoustic velocity

The DSI tool measures the transit times between sonic transmitters and an array of eight receivers. It averages replicate measurements, thus providing a direct measurement of sound velocity through sediments that is relatively free from the effects of formation damage and borehole enlargement (Schlumberger, 1989). The tool contains the monopole transmitters found on most sonic tools but also has two crossed dipole transmitters, providing shear wave velocity measurement in addition to the compressional wave velocity, even in the slow formations typically encountered during IODP expeditions.

## Formation MicroScanner

The FMS provides high-resolution electrical resistivity-derived images of the borehole (~30% of a 25 cm diameter borehole on each pass). The vertical resolution of FMS images is ~5 mm, allowing features such as clasts, thin beds, and bioturbation to be imaged. The resistivity measurements are converted to color or grayscale images for display. The tool uses four orthogonal imaging pads, each containing 16 button electrodes that are pressed against the borehole wall during the recording. A focused current is emitted from the button electrodes into the formation, with a return electrode near the top of the tool. The intensity of current passing through the button electrodes is measured and converted to an image. With the FMS tool, features such as bedding, fracturing, slump folding, and bioturbation can be resolved, and spatially oriented images allow fabric analysis and bed orientations to be measured (Luthi, 1990; Lovell et al., 1998; Salimullah and Stow, 1992). The maximum extension of the caliper arms is 15 in, so in holes or parts of holes where the diameter is larger the pad contact will be inconsistent and the FMS images may appear out of focus and too conductive. Irregularity in the borehole walls will also adversely affect the image quality if it leads to poor pad/wall contact.

Local contrasts in FMS images can be improved by applying dynamic and static normalizations to the FMS data. A linear gain was applied, which kept a constant mean and standard deviation within a sliding window of ~1 m or the entire logged interval, respectively. FMS images were oriented to magnetic north using the GPIT. This method allowed the dip and strike of geological features intersecting the hole to be measured from processed FMS images.

## Accelerometry and magnetic field measurement

Three-component acceleration and magnetic field measurements are made with the GPIT. The primary purpose of this tool, which incorporates a three-component accelerometer and a three-component magnetometer, is to determine the acceleration and orientation of the FMS-sonic tool string during logging. This provides a means of correcting the FMS images for irregular tool motion, allowing the true dip and direction (azimuth) of structures to be determined.

## Wireline logging data quality

Logging data quality may be seriously degraded by changes in the hole diameter and in sections where the borehole diameter greatly decreases or is washed out. Deep-investigation measurements such as resistivity and sonic velocity are least sensitive to borehole conditions. Nuclear measurements (density and neutron porosity) are more sensitive because of their shallower depth of investigation and the effect of drilling fluid volume on neutron and gamma ray attenuation. Corrections can be applied to the original data to reduce these effects. HNGS and SGT data provide a depth correlation between logging runs. Logs from different tool strings may, however, still have depth mismatches caused by either cable stretch or ship heave during recording.

## Logging depth scales

The depth of the wireline-logged measurement is determined from the length of the logging cable played out at the winch on the ship. The seafloor is identified on the natural gamma log by the abrupt reduction in gamma ray count at the water/sediment boundary (mudline). Discrepancies between the driller's depth and the wireline logging depth occur because of incomplete heave compensation, tidal changes, and cable stretch (~1 m/km) in the case of logging depth. The small differences between drill pipe depth and logging depth, and the even more significant discrepancy between IODP curation depth and logging depth, should be taken into account when using the logs for correlation between core and logging data. Core measurements such as susceptibility and density can be correlated with the equivalent downhole logs using the Sagan program, which allows linear shifting of the core depths onto the logging depth scale.

## Logging data flow and processing

After logging was completed in each hole, data were transferred to the shipboard downhole measurements laboratory for preliminary processing and interpretation. FMS image data were interpreted using Schlumberger's Geoframe (version 4.0.4.1) software package. Logging data were also transmitted onshore for processing soon after each hole was logged. Onshore data processing consisted of

- Depth-shifting all logs relative to a common datum (i.e., in mbsf),

- Corrections specific to individual tools, and

- Quality control and rejection of unrealistic or spurious values.

Once processed onshore, the data were transmitted back to the ship, providing final processed logging results during the expedition. Processed data were then replotted on board (see "Downhole Measurements" in each site chapter). Postcruise-processed data in ASCII format are available directly from the IODP U.S. Implementing Organization (USIO) Science Services LDEO World Wide Web site at **iodp.ldeo.columbia.edu/DATA/IODP/index.html.**

# References

Aguirre, E., and Pasini, G., 1985. The Pliocene–Pleistocene boundary. *Episodes,* 8:11–120.

Altenbach, A.V., Lutze, G.F., Schiebel, R., and Schönfeld, J., 2003. Impact of interrelated and independent ecological controls on benthic foraminifera: an example from the Gulf of Guinea. *Paleogeogr., Paleoclimatol., Paleoecol.,* 197:213–238. **doi:10.1016/S0031-0182(03)00463-2**

Baldauf, J.G., 1985. Cenozoic diatom biostratigraphy and paleoceanography of the Rockall Plateau region, North Atlantic, Deep Sea Drilling Project Leg 81. *In* Roberts, D.G., Schnitker, D., et al., *Init. Repts. DSDP,* 81: Washington (U.S. Govt. Printing Office), 439–478.

Balsam, W.L., and Damuth, J.E., 2000. Further investigations of shipboard vs. shore-based spectral data: implications for interpreting Leg 164 sediment composition. *In* Paull, C.K., Matsumoto, R., Wallace, P., and Dillon, W.P. (Eds.), *Proc. ODP, Sci. Results,* 164: College Station, TX (Ocean Drilling Program), 313–324. [**HTML**]

Balsam, W.L., Damuth, J.E., and Schneider, R.R., 1997. Comparison of shipboard vs. shore-based spectral data from Amazon-Fan cores: implications for interpreting sediment composition. *In* Flood, R.D., Piper, D.J.W., Klaus, A., and Peterson, L.C. (Eds.), *Proc. ODP, Sci. Results,* 155: College Station, TX (Ocean Drilling Program), 193–215. [**PDF**]

Balsam, W.L., Deaton, B.C., and Damuth, J.E., 1998. The effects of water content on diffuse reflectance measurements of deep-sea core samples: an example from ODP Leg 164 sediments. *Mar. Geol.,* 149:177–189. **doi:10.1016/S0025-3227(98)00033-4**

Barron, J., 1985. Late Eocene to Holocene diatom biostratigraphy of the equatorial Pacific Ocean, Deep Sea Drilling Project Leg 85. *In* Mayer, L., Theyer, F., Thomas, E., et al., *Init. Repts. DSDP,* 85: Washington (U.S. Govt. Printing Office), 413–456.

Berggren, W.A., Kent, D.V., Flynn, J.J., and van Couvering, J.A., 1985. Cenozoic geochronology. *Geol. Soc. Am. Bull.* 96:1407–1418. **doi:10.1130/0016-7606(1985)96<1407:CG>2.0.CO;2**

Blum, P., 1997. Physical properties handbook: a guide to the shipboard measurement of physical properties of deep-sea cores. *ODP Tech. Note,* 26 [Online]. Available from World Wide Web: **<http://www-odp.tamu.edu/publications/tnotes/tn26/INDEX.HTM>.**

Burckle, L.H., 1972. Late Cenozoic planktonic diatom zones from the eastern equatorial Pacific. *In* Simonsen, R. (Ed.), *First Symposium on Recent and Fossil Marine Diatoms.* Nova Hedwegia Beih., 39:217–246.

Burckle, L.H., 1977. Neogene diatom correlations in the Circum-Pacific. *Proc. 1st Int. Congress Pacific Neogene Stratigraphy,* 36–39.

Cande, S.C., and Kent, D.V., 1995. Revised calibration of the geomagnetic polarity timescale for the Late Cretaceous and Cenozoic. *J. Geophys. Res.,* 100:6093–6095. **doi:10.1029/94JB03098**

Channell, J.E.T., Labs, J., and Raymo, M.E., 2003. The Reunion Subchronozone at ODP Site 981 (Feni Drift, North Atlantic). *Earth Planet. Sci. Lett.,* 215:1–12.

Channell, J.E.T., Mazaud, A., Sullivan, P., Turner, S., and Raymo, M.E., 2002. Geomagnetic excursions and paleointensities in the Matuyama Chron at ODP Sites 983 and 984 (Iceland Basin). *J. Geophys. Res.,* 107. **doi:10.1029/2001JB000491**

Curry, W.B., Shackleton, N.J., Richter, C., et al., 1995. *Proc. ODP, Init. Repts.,* 154: College Station, TX (Ocean Drilling Program).

de Vernal, A., and Mudie, P.J., 1989a. Late Pliocene to Holocene palynostratigraphy at ODP Site 645, Baffin Bay. *In* Srivastava, S.P., Arthur, M.A., Clement, B., et al., *Proc. ODP, Sci. Results,* 105: College Station, TX (Ocean Drilling Program), 387–399. [**PDF**]

de Vernal, A., and Mudie, P.J., 1989b. Pliocene and Pleistocene palynostratigraphy at ODP Sites 646 and 647, eastern and southern Labrador Sea. *In* Srivastava, S.P., Arthur, M.A., Clement, B., et al., *Proc. ODP, Sci. Results,* 105: College Station, TX (Ocean Drilling Program), 401–422. [**PDF**]

de Vernal, A., and Mudie, P.J., 1992. Pliocene and Quaternary dinoflagellate cyst stratigraphy in Labrador Sea: paleoecological implications. *In* Head, M.J., and Wrenn, J.H. (Eds.), *Neogene and Quaternary Dinoflagellate Cysts and Acritarchs:* Salt Lake City (Publisher's Press), 329–346.

de Vernal, A., Londeix, L., Mudie, P.J., Harland, R., Morzadec-Kerfourn, M.T., Turon, J.-L., and Wrenn, J.H., 1992. Quaternary organic-walled dinoflagellate cysts of the North Atlantic Ocean and adjacent seas: ecostratigraphy and biostratigraphy. *In* Head, M.J., and Wrenn, J.H. (Eds.), *Neogene and Quaternary Dinoflagellate Cysts and Acritarchs:* Salt Lake City (Publisher's Press), 289–328.

Droser, M.L., and Bottjer, D.J., 1986. A semiquantitative field classification of ichnofabric. *J. Sediment. Petrol.,* 56:558–559.

Ellis, D.V., 1987. *Well Logging for Earth Scientists:* New York (Elsevier).

Evans, 1965. GRAPE—A device for continuous determination of material density and porosity. *SPWL, 6th Ann. Symposium,* 2:25.

Gersonde, R., Hodell, D.A., Blum, P., et al., 1999. *Proc. ODP, Init. Repts.,* 177 [CD-ROM]. Available from: Ocean Drilling Program, Texas A&M University, College Station, TX 77845-9547, U.S.A. [HTML]

Gieskes, J.M., Gamo, T., and Brumsack, H., 1991. Chemical methods for interstitial water analysis aboard *JOIDES Resolution. ODP Tech. Note,* 15 [Online]. Available from World Wide Web: <http://www-odp.tamu.edu/publications/tnotes/tn15/f_chem1.htm>.

Goldberg, D., 1990. Test performance of the Ocean Drilling Program wireline heave motion compensator. *Sci. Drill.,* 1:206–209.

Goldberg, D., 1997. The role of downhole measurements in marine geology and geophysics. *Rev. Geophys.,* 35:315–342. doi:10.1029/97RG00221

Goll, R.M., and Bjørklund, K.R., 1989. A new radiolarian biostratigraphy for the Neogene of the Norwegian Sea: ODP Leg 104. *In* Eldholm, O., Thiede, J., Taylor, E., et al., *Proc. ODP, Sci. Results,* 104: College Station, TX (Ocean Drilling Program), 697–737. [PDF]

Hagelberg, T., Shackleton, N., Pisias, N., and Shipboard Scientific Party, 1992. Development of composite depth sections for Sites 844 through 854. *In* Mayer, L., Pisias, N., Janecek, T., et al., *Proc. ODP, Init. Repts.,* 138 (Pt. 1): College Station, TX (Ocean Drilling Program), 79–85.

Hagelberg, T.K., Pisias, N.G., Shackleton, N.J., Mix, A.C., and Harris, S., 1995. Refinement of a high-resolution, continuous sedimentary section for studying equatorial Pacific Ocean paleoceanography, Leg 138. *In* Pisias, N.G., Mayer, L.A., Janecek, T.R., Palmer-Julson, A., and van Andel, T.H. (Eds.), *Proc. ODP, Sci Results,* 138: College Station, TX (Ocean Drilling Program), 31–46.

Harland, R., 1979. Dinoflagellate biostratigraphy of Neogene and Quaternary sediments at Holes 400/400A in the Bay of Biscay (Deep Sea Drilling Project Leg 48). *In* Montadert, L., Roberts, D.G., et al., *Init. Repts. DSDP,* 48: Washington (U.S. Govt. Printing Office), 531–545.

Harms, J.C., and Choquette, P.W., 1965. Geologic evaluation of a gamma-ray porosity device. *Trans. SPWLA 6th Ann. Logging Symp.:* Dallas, C1–C37.

Hayward, B.W., 2001. Global deep-sea extinctions during the Pleistocene ice-ages. *Geology,* 29:599–602. doi:10.1130/0091-7613(2001)029<0599:GDSEDT>2.0.CO;2

Head, M.J., 1998a. Marine environmental change in the Pliocene and early Pleistocene of eastern England: the dinoflagellate evidence reviewed. *Meded. Ned. Inst. Toegepaste Geowet. TNO,* 60:199–226.

Head, M.J., 1998b. Pollen and dinoflagellates from the Red Crag at Walton-on-the-Naze, Essex: evidence for a mild climatic phase during the early late Pliocene of eastern England. *Geol. Mag.,* 135:803–817. doi:10.1017/S0016756898001745

Head, M.J., and Norris, G., 2003. New species of dinoflagellate cysts and other palynomorphs from the late Neogene of the western North Atlantic, DSDP Hole 603C. *J. Paleontol.,* 77:1–15.

Head, M.J., and Westphal, H., 1999. Palynology and paleoenvironments of a Pliocene carbonate platform: the Clino Core, Bahamas. *J. Paleontol.,* 73:1–25.

Head, M.J., Norris, G., and Mudie, P.J., 1989a. Palynology and dinocyst stratigraphy of the Miocene in ODP Leg 105, Hole 645E, Baffin Bay. *In* Srivastava, S.P., Arthur, M.A., Clement, B., et al., *Proc. ODP, Sci. Results,* 105: College Station, TX (Ocean Drilling Program), 467–514. [PDF]

Head, M.J., Norris, G., and Mudie, P.J., 1989b. Palynology and dinocyst stratigraphy of the upper Miocene and lowermost Pliocene, ODP Leg 105, Site 646, Labrador Sea. *In* Srivastava, S.P., Arthur, M.A., Clement, B., et al., *Proc. ODP, Sci. Results,* 105: College Station, TX (Ocean Drilling Program), 423–451. [PDF]

Head, M.J., Riding, J.B., Eidvin, T., and Chadwick, R.A., 2004. Palynology and foraminiferal biostratigraphy of (Upper Pliocene) Nordland Group mudstones at Sleipner, northern North Sea. *Mar. Petrol. Geol.,* 21:277–297. doi:10.1016/j.marpetgeo.2003.12.002

Jansen, E., Raymo, M.E., Blum, P., et al., 1996. *Proc. ODP, Init. Repts.,* 162: College Station, TX (Ocean Drilling Program).

Jorissen, F.J., de Stigter, H.C., and Widmark, J.G.V., 1995. A conceptual model explaining benthic foraminiferal microhabitats. *Mar. Micropaleontol.,* 26:3–15. doi:10.1016/0377-8398(95)00047-X

Kennett, J.P., and Srinivasan, M.S., 1983. *Neogene Planktonic Foraminifera: A Phylogenetic Atlas:* Stroudsburg, PA (Hutchinson Ross).

Koç, N., Hodell, D.A., Kleiven, H., and Labeyrie, L., 1999. High-resolution Pleistocene diatom biostratigraphy of Site 983 and correlations with isotope stratigraphy. *In* Raymo, M.E., Jansen, E., Blum, P., and Herbert, T.D. (Eds.), 1999. *Proc. ODP, Sci. Results,* 162: College Station, TX (Ocean Drilling Program), 51–62. [HTML]

Lamont-Doherty Earth Observatory-Borehole Research Group, 2001. *Wireline Logging Services Guide* [Online]. Available from World Wide Web: <http://www.ldeo.columbia.edu/BRG/ODP/LOGGING/>.

Loeblich, A.R., and Tappan, H., 1988. *Foraminiferal Genera and Their Classification* (Vol. 2): New York (Van Nostrand Reinhold Co.).

Louwye, S., Head, M.J., and De Schepper, S., 2004. Dinoflagellate cyst stratigraphy and palaeoecology of the Pliocene in northern Belgium, southern North Sea Basin. *Geol. Mag.,* 141:353–378. doi:10.1017/S0016756804009136

Lovell, M.A., Harvey, P.K., Brewer, T.S., Williams, C., Jackson, P.D., and Williamson, G., 1998. Application of FMS images in the Ocean Drilling Program: an overview. *In* Cramp, A., MacLeod, C.J., Lee, S.V., and Jones, E.J.W. (Eds.), *Geological Evolution of Ocean Basins: Results from the Ocean Drilling Program.* Geol. Soc. Spec. Publ., 131:287–303.

Luthi, S.M., 1990. Sedimentary structures of clastic rocks identified from electrical borehole images. *In* Hurst, A., Lovell, M.A., and Morton, A.C. (Eds.), *Geological Applications of Wireline Logs.* Spec. Publ.—Geol. Soc. London, 48:3–10.

Lyle, M., Koizumi, I., Richter, C., et al., 1997. *Proc. ODP, Init. Repts.,* 167 [Online]. Available from World Wide Web: <http://www-odp.tamu.edu/publications/167_IR/167TOC.HTM>.

Manheim, F.T., and Sayles, F.L., 1974. Composition and origin of interstitial waters of marine sediments, based on deep sea drill cores. *In* Goldberg, E.D. (Ed.), *The Sea* (Vol. 5): *Marine Chemistry: The Sedimentary Cycle:* New York (Wiley), 527–568.

Manum, S.V., Boulter, M.C., Gunnarsdottir, H., Rangnes, K., and Scholze, A., 1989. Eocene to Miocene palynology of the Norwegian Sea (ODP Leg 104). *In* Eldholm, O., Thiede, J., et al., *Proc. ODP, Sci. Results,* 104: College Station, TX (Ocean Drilling Program), 611–662. [PDF]

Martini, E., 1971. Standard Tertiary and Quaternary calcareous nannoplankton zonation. *In* Farinacci, A. (Ed.), *Proc. 2nd Int. Conf. Planktonic Microfossils Roma:* Rome (Ed. Tecnosci.), 2:739–785.

Matthiessen, J., and Brenner, W., 1996. Dinoflagellate cyst ecostratigraphy of Pliocene–Pleistocene sediments from the Yermak Plateau (Arctic Ocean, Hole 911A). *In* Thiede, J., Myhre, A.M., Firth, J.V., Johnson, G.L., and Ruddiman, W.F. (Eds.), *Proc. ODP, Sci. Results,* 151: College Station, TX (Ocean Drilling Program), 243–253.

Mazzullo, J.M., Meyer, A., and Kidd, R.B., 1988. New sediment classification scheme for the Ocean Drilling Program. *In* Mazzullo, J.M., and Graham, A.G. (Eds.), Handbook for shipboard sedimentologists. *ODP Tech. Note,* 8:45–67.

Mix, A.C., Tiedemann, R., Blum, P., et al., 2003. *Proc. ODP, Init. Repts.,* 202 [Online]. Available from World Wide Web: <http://www-odp.tamu.edu/publications/202_IR/202ir.htm>.

Moran, K., 1997. Elastic property corrections applied to Leg 154 sediment, Ceara Rise. *In* Shackleton, N.J., Curry, W.B., Richter, C., and Bralower, T.J. (Eds.), *Proc. ODP, Sci. Results,* 154: College Station, TX (Ocean Drilling Program), 151–155. [PDF]

Mudie, P.J., 1987. Palynology and dinoflagellate biostratigraphy of Deep Sea Drilling Project Leg 94, Sites 607 and 611, North Atlantic Ocean. *In* Ruddiman, W.F., Kidd, R.B., Thomas, E., et al., *Init. Repts. DSDP,* 94 (Pt. 2): Washington (U.S. Govt. Printing Office), 785–812.

Mudie, P.J., 1989. Palynology and dinocyst biostratigraphy of the late Miocene to Pleistocene, Norwegian Sea: ODP Leg 104, Sites 642–644. *In* Eldholm, O., Thiede, J., Taylor, E., et al., *Proc. ODP, Sci. Results,* 104: College Station, TX (Ocean Drilling Program), 587–610.

Munsell Color Company, Inc., 1994. *Munsell Soil Color Chart* (Revised ed.): Newburgh, MD (Munsell Color).

Murray, R.W., Miller, D.J., and Kryc, K.A., 2000. Analysis of major and trace elements in rocks, sediments, and interstitial waters by inductively coupled plasma–atomic emission spectrometry (ICP-AES). *ODP Tech. Note,* 29 [Online]. Available from World Wide Web: <http://www-odp.tamu.edu/publications/tnotes/tn29/INDEX.HTM>.

Piasecki, S., 2003. Neogene dinoflagellate cysts from Davis Strait, offshore west Greenland. *Mar. Petrol. Geol.,* 20:1075–1088. doi:10.1016/S0264-8172(02)00089-2

Pimmel, A., and Claypool, G., 2001. Introduction to shipboard organic geochemistry on the *JOIDES Resolution. ODP Tech. Note,* 30 [Online]. Available from World Wide Web: <http://www-odp.tamu.edu/publications/tnotes/tn30/INDEX.HTM>.

Poulsen, N.E., Manum, S.B., Williams, G.L., and Ellegaard, M., 1996. Tertiary dinoflagellate biostratigraphy of Sites 907, 908, and 909 in Norwegian-Greenland Sea. *In* Thiede, J., Myhre, A.M., Firth, J.V., Johnson, G.L., and Ruddiman, W.F. (Eds.), *Proc. ODP, Sci. Results,* 151: College Station, TX (Ocean Drilling Program), 255–287.

Powell, A.J. (Ed.), 1992. *A Stratigraphic Index of Dinoflagellate Cysts:* London (Chapman and Hall).

Powell, A.J., 1988. A preliminary investigation in the Neogene dinoflagellate cyst biostratigraphy of the British Southwestern Approaches. *Bull. Cent. Rech. Explor.-Prod. Elf-Aquitaine,* 12:277–311.

Rider, M.H., 1996. *The Geological Interpretation of Well Logs* (2nd ed.): Caithness (Whittles Publishing).

Ruddiman, W.F., Cameron, D., and Clement, B.M., 1987. Sediment disturbance and correlation of offset holes drilled with the hydraulic piston corer: Leg 94. *In* Ruddiman, W.F., Kidd, R.B., Thomas, E., et al., *Init. Repts. DSDP,* 94 (Pt. 2): Washington (U.S. Govt. Printing Office), 615–634.

Salimullah, A.R.M., and Stow, D.A.V., 1992. Application of FMS images in poorly recovered coring intervals: examples from ODP Leg 129. *In* Hurst, A., Griffiths, C.M., and Worthington, P.F. (Eds.), *Geological Application of Wireline Logs II.* Geol. Soc. Spec. Publ., 65:71–86.

Sato, T., Kameo, K., and Mita, I., 1999. Validity of the latest Cenozoic calcareous nannofossil datums and its application to the tephrochronology. *Earth Sci.,* 53:265–274.

Schlumberger, 1989. *Log Interpretation Principles/Applications:* Houston (Schlumberger Educ. Services), SMP–7017.

Schlumberger, 1994. *Log Interpretation Charts:* Sugarland, TX (Schlumberger Wireline and Testing), SMP-7006.

Schrader, H.J., and Gersonde, R., 1978. Diatoms and silicoflagellates. *In* Zachariasse, W.J., et al. (Eds.), *Micropaleontological Counting Methods and Techniques: An Exercise of an Eight Metres Section of the Lower Pliocene of Cap Rossello, Sicily.* Utrecht Micropaleontol. Bull., 17:129–176.

Schultheiss, P.J., and McPhail, S.D., 1989. An automated *P*-wave logger for recording fine-scale compressional wave velocity structures in sediments. *In* Ruddiman, W., Sarnthein, M., et al., *Proc. ODP, Sci. Results,* 108: College Station, TX (Ocean Drilling Program), 407–413. [PDF]

Serra, O., 1984. *Fundamentals of Well-Log Interpretation* (Vol. 1): *The Acquisition of Logging Data:* Dev. Pet. Sci., 15A: Amsterdam (Elsevier).

Serra, O., 1986. *Fundamentals of Well-Log Interpretation* (Vol. 2): *The Interpretation of Logging Data.* Dev. Pet. Sci., 15B: Amsterdam (Elsevier).

Serra, O., 1989. *Formation MicroScanner Image Interpretation:* Houston (Schlumberger Educ. Services), SMP-7028.

Shipboard Scientific Party, 2003. Explanatory notes. *In* Mix, A.C., Tiedemann, R., Blum, P., et al., *Proc. ODP, Init. Repts.,* 202, 1–76 [CD_ROM]. Available from: Ocean Drilling Program, Texas A&M University, College Station TX 77845-9547, USA. [HTML]

Spencer-Cervato, C., and Thierstein, H.R., 1997. First appearance of *Globorotalia truncatulinoides;* cladogenesis and immigration. *Mar. Micropaleontol.,* 30:267–291. doi:10.1016/S0377-8398(97)00004-2

Takayama, T., and Sato, T., 1987. Coccolith biostratigraphy of the North Atlantic Ocean, Deep Sea Drilling Project Leg 94. *In* Ruddiman, W.F., Kidd, R.B., Thomas, E., et al., *Init. Repts. DSDP,* 94 (Pt. 2): Washington (U.S. Govt. Printing Office), 651–702.

Takayama, T., and Sato, T., 1993–1995. Coccolith biostratigraphy of the Pliocene/Pleistocene boundary stratotype. *Ann. Geol. Pays Hell.,* 36:143–150.

Thomas, R.G., Guyodo, Y., and Channell, J.E.T., 2003. U channel track for susceptibility measurements. *Geochem., Geophys., Geosyst.,* 4(6). doi:10.1029/2002GC000454

Wang, P., Prell, W.L., Blum, P., et al., 2000. *Proc. ODP, Init. Repts.,* 184 [Online]. Available from World Wide Web: <http://www-odp.tamu.edu/publications/184_IR/184ir.htm>.

Weaver, P.P.E., and Clement, B.M., 1987. Magnetobiostratigraphy of planktonic foraminiferal datums, DSDP Leg 94, North Atlantic. *In* Ruddiman, W.F., Kidd, R.B., Thomas, E., et al., *Init. Repts. DSDP,* 94: Washington (U.S. Govt. Printing Office), 815–829.

Wentworth, C.K., 1922. A scale of grade and class terms of clastic sediments. *J. Geol.,* 30:377–392.

Williams, G.L., Lentin, J.K., and Fensome, R.A., 1998. *The Lentin and Williams Index of Fossil Dinoflagellate Cysts* (1998 ed.). Am. Assoc. Stratigr. Palynol., Contrib. Ser., Vol. 34.

Zachos, J.C., Kroon, D., Blum, P., et al., 2004. *Proc. ODP, Init. Repts.,* 208 [Online]. Available from World Wide Web: <http://www-odp.tamu.edu/publications/208_IR/208ir.htm>.

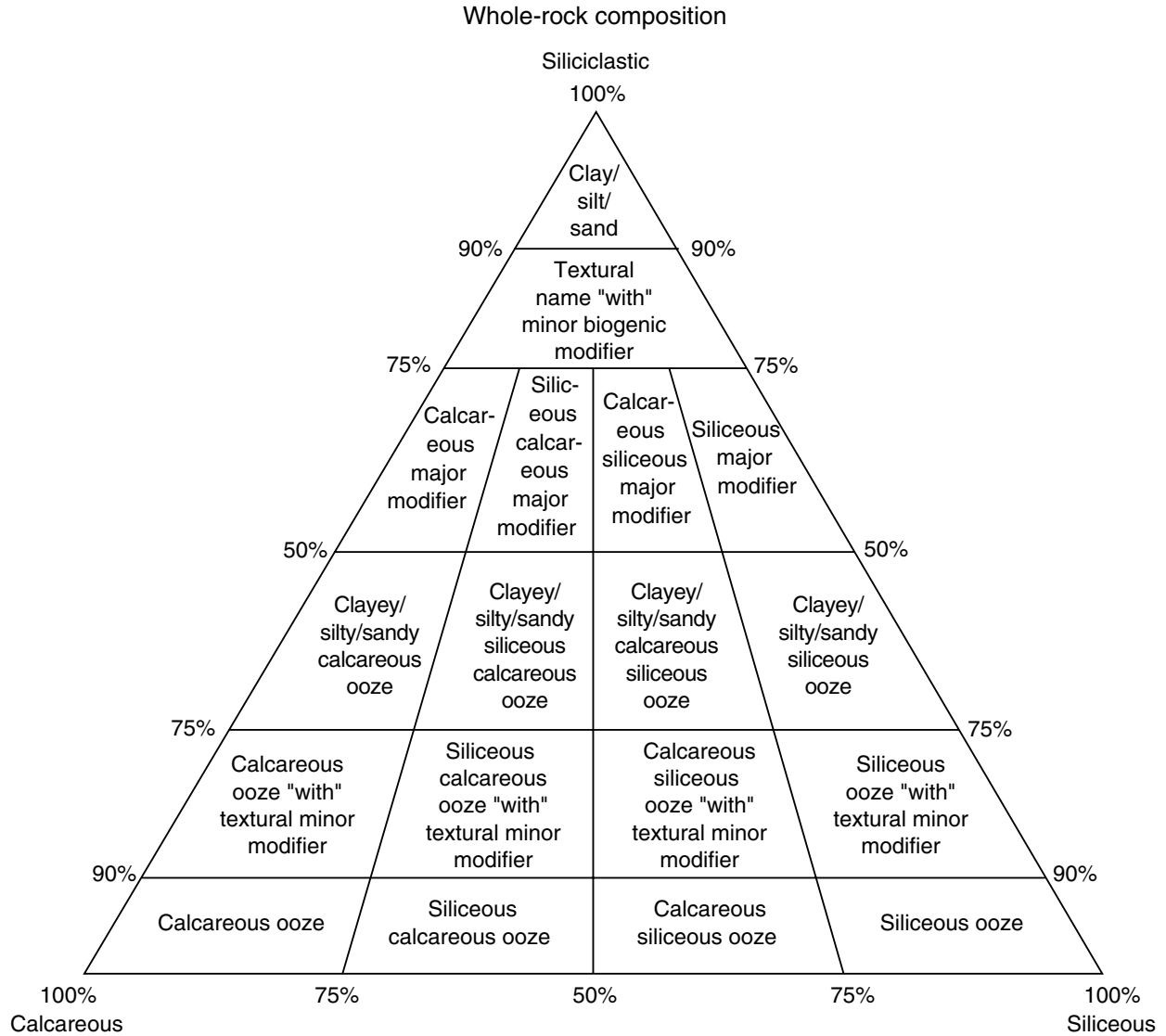**Figure F1.** Ternary diagram showing nomenclature for principal components of whole-sediment composition.

**Figure F2.** Grain-size classification scheme of Wentworth (1922).

| Grain size (mm) | Grain size (µm) | Phi (φ) | Wentworth size class | | Rock type |
|---|---|---|---|---|---|
| 4096 | | -12.0 | Boulder | | |
| 256 | | -8.0 | Cobble | | |
| 64 | | -6.0 | Pebble | Gravel | Conglomerate/Breccia |
| 4 | | -2.0 | Granule | | |
| 2.00 | | -1.0 | Very coarse sand | | |
| 1.00 | | 0.0 | Coarse sand | | |
| 1/2   0.50 | 500 | 1.0 | Medium sand | Sand | Sandstone |
| 1/4   0.25 | 250 | 2.0 | Fine sand | | |
| 1/8   0.125 | 125 | 3.0 | Very fine sand | | |
| 1/16   0.0625 | 63 | 4.0 | Coarse silt | | |
| 1/32   0.031 | 31 | 5.0 | Medium silt | | |
| 1/64   0.0156 | 15.6 | 6.0 | Fine silt | Silt | Siltstone |
| 1/128   0.0078 | 7.8 | 7.0 | Very fine silt | | |
| 1/256   0.0039 | 3.9 | 8.0 | Clay | Mud | Claystone |
| 0.00006 | 0.06 | 14.0 | | | |

**Figure F3.** Ternary diagram showing nomenclature for siliciclastic sediment components based on grain size.
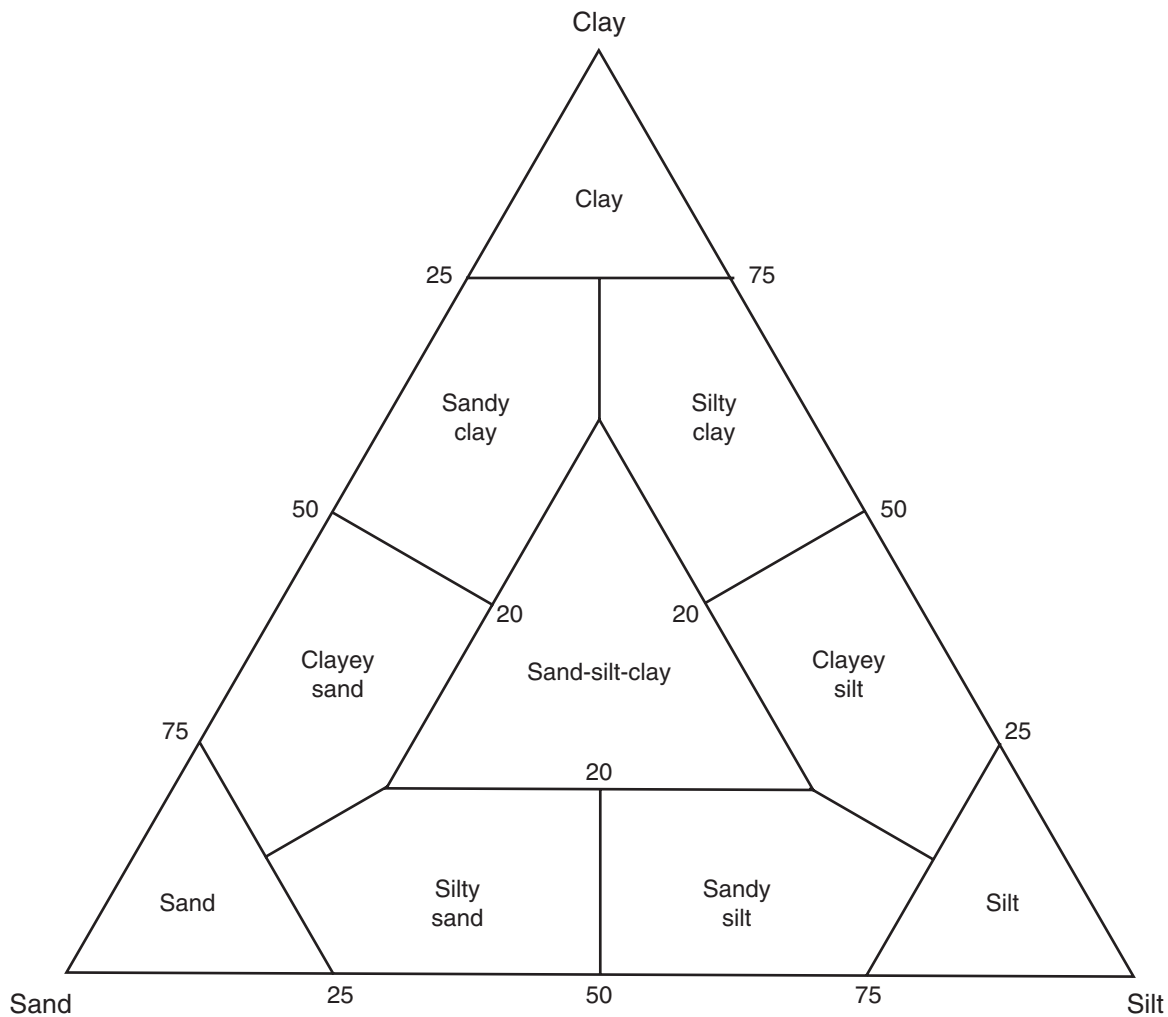
**Figure F4.** Example of an AppleCORE summary barrel sheet. SS = smear slide, IW = interstitial water, PAL = micropaleontology, dk GY = dark gray, GY = gray.
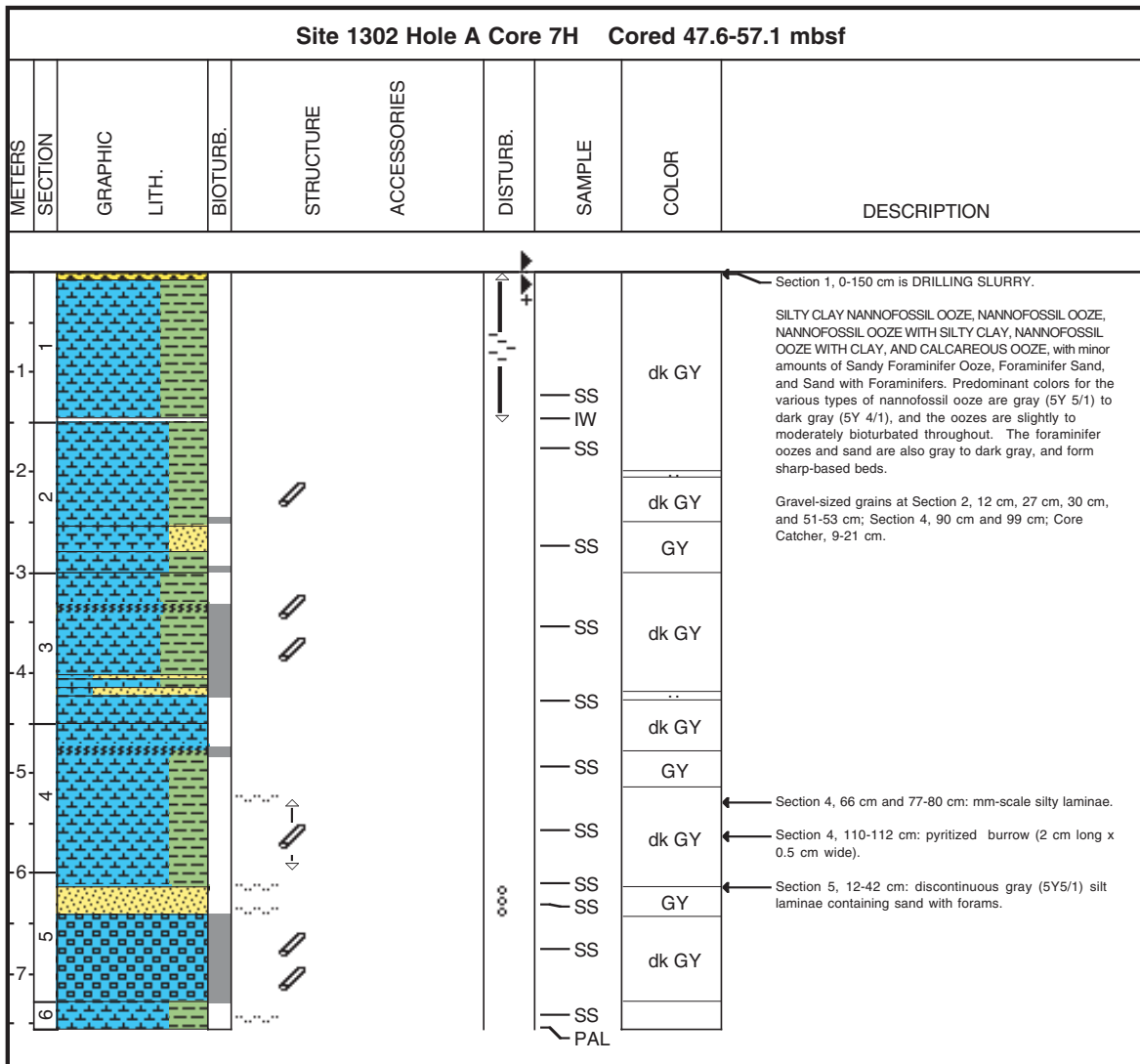
**Figure F5.** Key to symbols used for graphic lithologies.

Siliciclastic Sediments

Sand or sandstone

Silty sand

Clayey sand

Silt or siltstone

Sandy silt

Clayey silt

Silty clay

Clay or claystone

Sand-silt-clay

Gravel

Conglomerate

Pelagic Sediments

Nannofossil ooze

Foraminifer ooze

Calcareous ooze

Diatom ooze

Diatom-radiolarian ooze

Contacts

Sharp

Scoured

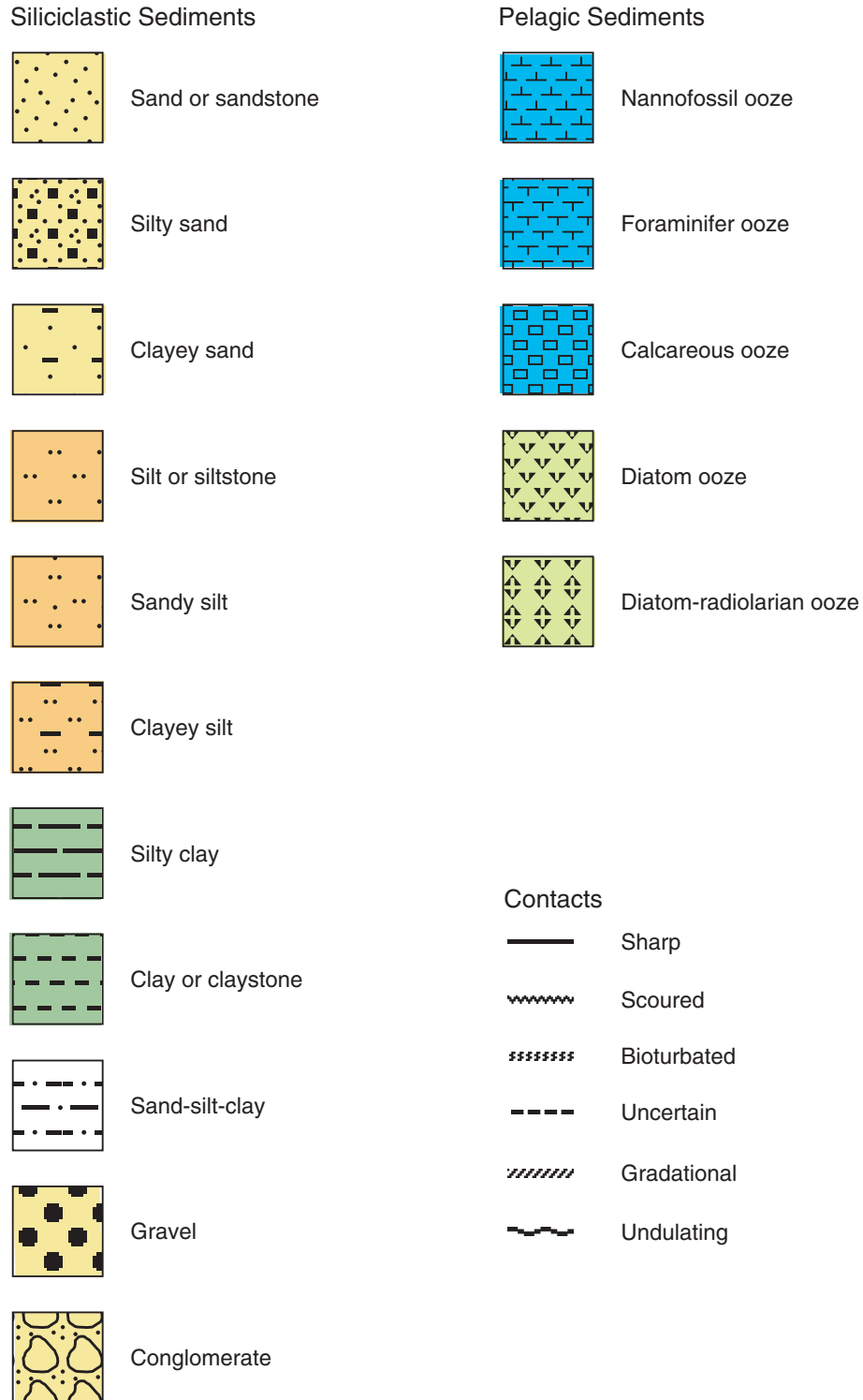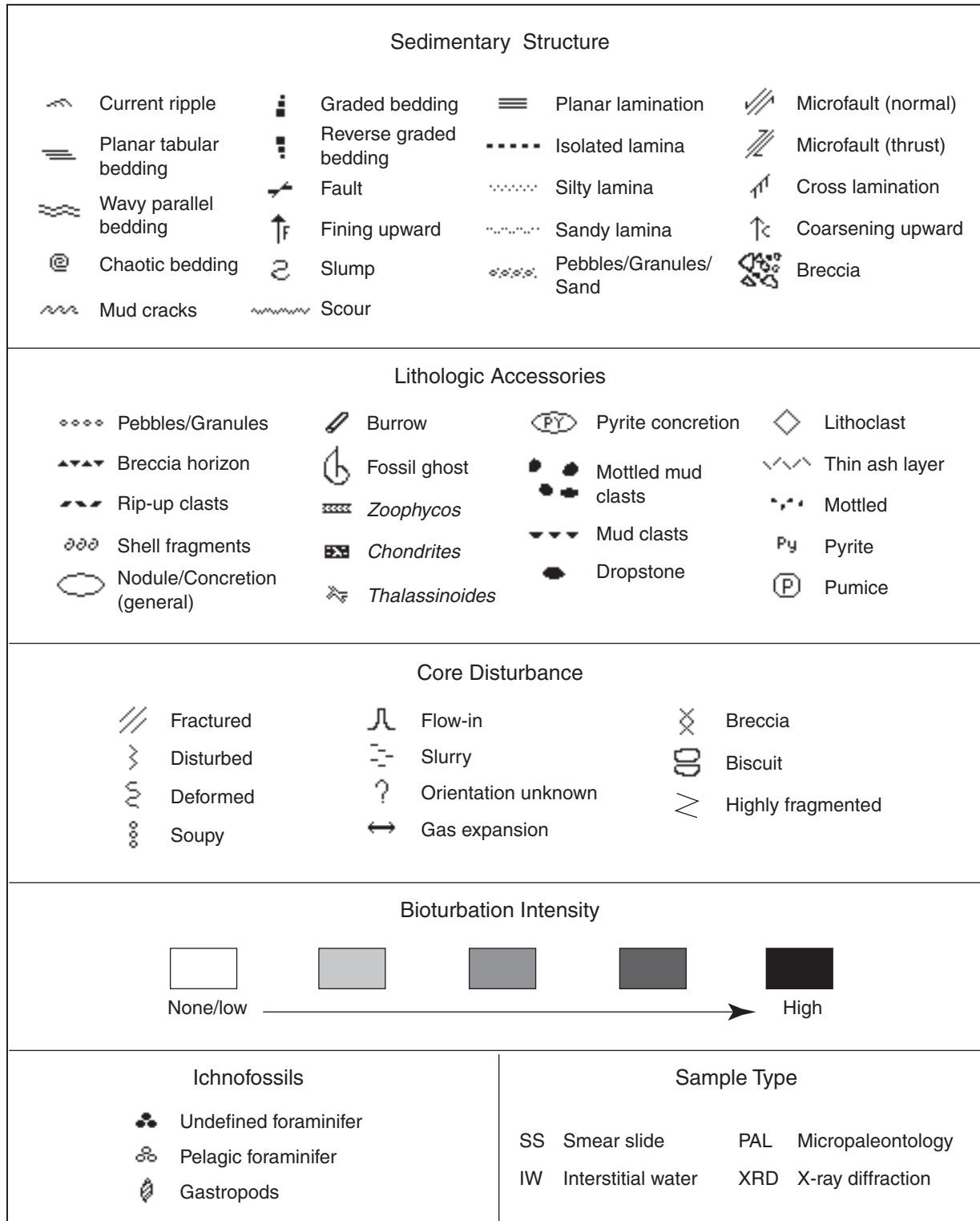Bioturbated

Uncertain

Gradational

Undulating

**Figure F6.** Key to other symbols used on the AppleCORE summary barrel sheets.

**Figure F7.** Correlation of geomagnetic polarity timescale (GPTS) (Cande and Kent, 1995), biostratigraphic zonation, and biohorizons used during Expedition 303. DSDP = Deep Sea Drilling Project, ODP = Ocean Drilling Program, LO = last occurrence, FO = first occurrence.
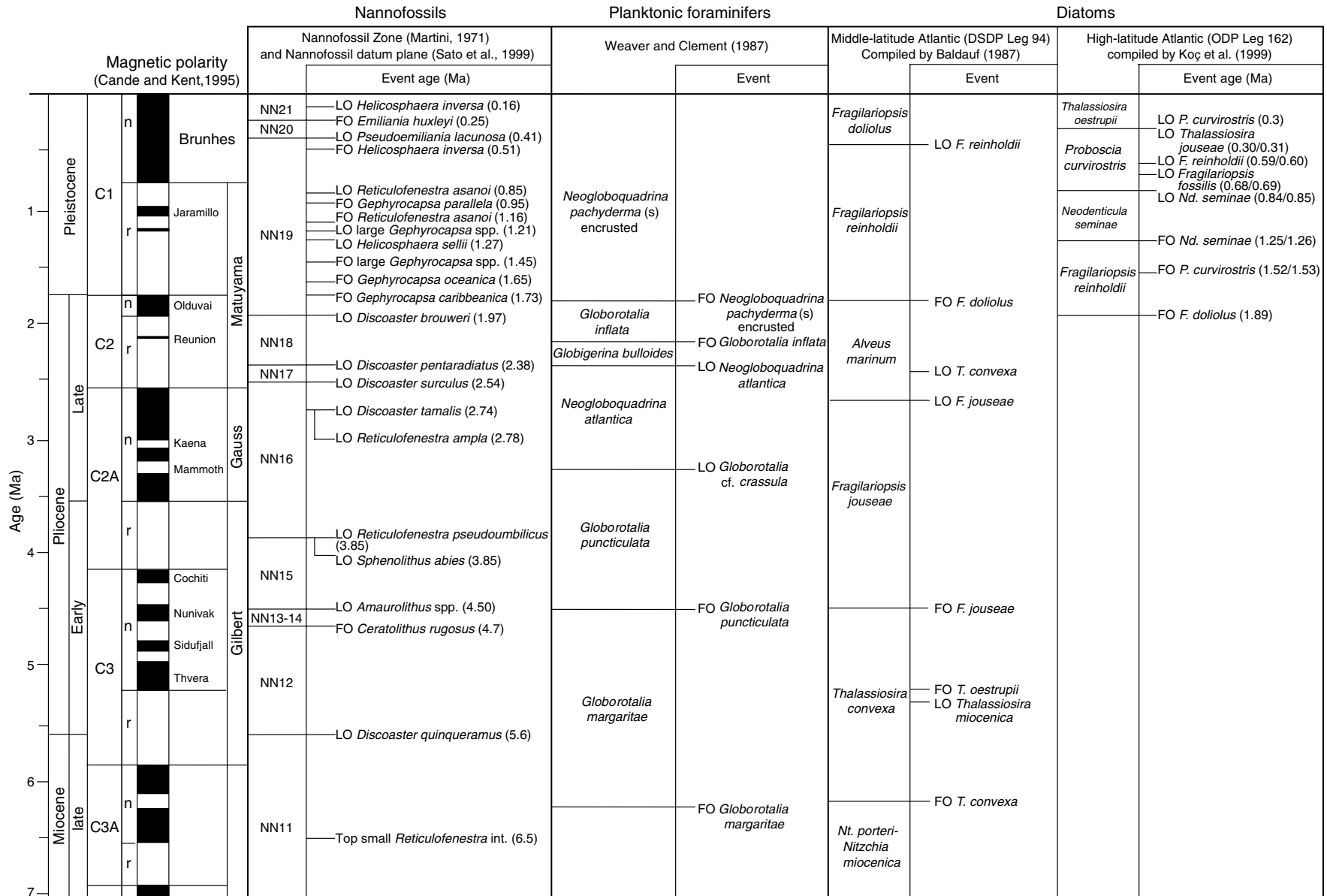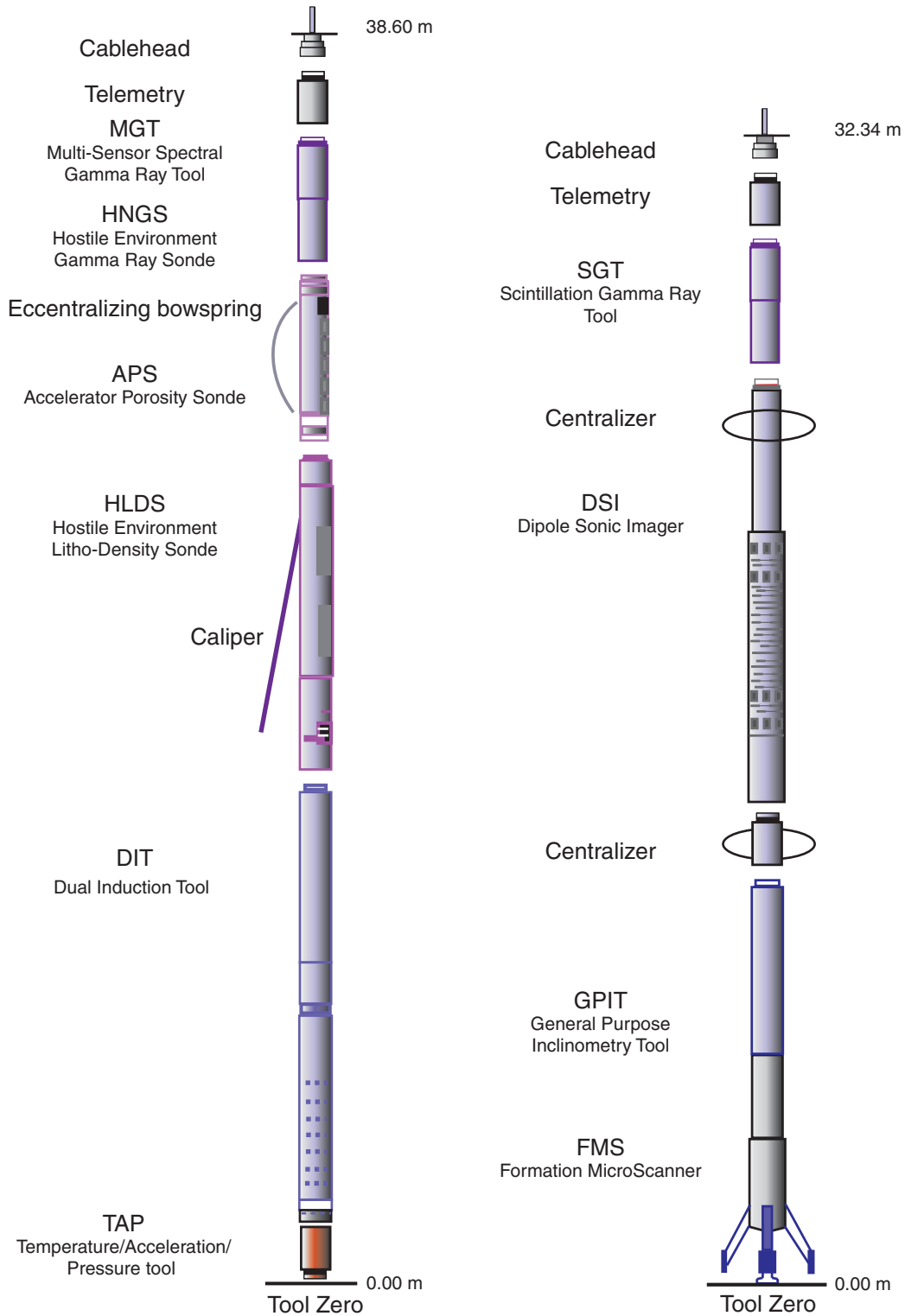
**Figure F8.** Configuration of the wireline logging tool strings that were used during Expedition 303.

**Table T1.** Radiolarian zonation used during Expedition 303.

| Epoch | North Atlantic zonation* | Event (bottom) | Age (Ma) BKV85 | Age (Ma) CK95 |
|---|---|---|---|---|
| Pleistocene | C. davisiana davisiana | FO C. davisiana davisiana | 0.0/2.6 | 0.0/2.7 |
| Pliocene | C. davisiana davisiana | FO C. davisiana davisiana | 0.0/2.6 | 0.0/2.7 |
| | Spongaster? tetras | FO S.? tetras | 2.6/2.9–3.1 | 2.7/3.0–3.2 |
| | Pseudodictyophimus gracilipes tetracanthus | FO P. gracilipes tetracanthus | 2.9–3.1/4.0 | 3.0–3.2/4.4 |
| | Antarctissa whitei | LO L. circus | 4.0/5.2 | 4.4/5.7 |
| late Miocene | Liriospyris circus | FO L. circus | 5.2/5.5 | 5.7/6.1 |
| | Tessarastrum thiedei | FO T. thiedei | 5.5/6.2 | 6.1/6.7 |
| | Larcospira bulbosa | FO L. bulbosa | 6.2/6.3–6.9 | 6.7/6.8–7.7 |
| | Hexalonche esmarki | FO H. esmarki | 6.3–6.9/7.7–7.9 | 6.8–7.7/8.5–8.6 |

Note: * = zonation from Goll and Bjørklund, 1989. FO = first occurrence, LO = last occurrence. BKV85 = Berggren et al., 1985, CK95 = Cande and Kent, 1995.

**Table T2.** Analytical methods and precisions for interstitial water geochemistry measurements, Expedition 303.

| Parameter | Method | Precision (%) |
|---|---|---|
| Alkalinity | Gran titration | 1.5 |
| pH | Gran titration | 3.1 |
| $Cl^-$ | Titration with $AgNO_3$ | 0.2 |
| $SO_4^{2-}$ | Ion chromatography | 2.0 |
| $Li^+$ | ICP-AES | 2.2 |
| $K^+$ | Ion chromatography | 1.6 |
| $NH_4^+$ | Spectrophotometer | 2.5 |
| $Mg^{2+}$ | Ion chromatography | 2.7 |
| $Ca^{2+}$ | Ion chromatography | 5.2 |
| $Sr^{2+}$ | ICP-AES | 1.3 |
| $Ba^{2+}$ | ICP-AES | 27.1 |
| $Mn^{2+}$ | ICP-AES | 27.0 |
| $Fe^{2+}$ | ICP-AES | 62.1 |
| $H_3BO_3$ | ICP-AES | 2.1 |
| $H_4SiO_4$ | ICP-AES | 3.9 |

Note: The reproducibility of analytical techniques is expressed as 1σ standard deviation of the mean of multiple determinations of a standard. The standard data used to calculate analytical precision in this table were generated during the period of analyses for the samples from Sites U1302–U1307. ICP-AES = inductively coupled plasma–atomic emission spectroscopy.

**Table T3.** Measurements and specifications for wireline tools.

| Tool string | Tool† | Measurement | Sampling interval (cm) | Approximate vertical resolution (cm) |
|---|---|---|---|---|
| Triple combination | MGT* | Gamma ray | 15 | 15 |
| | HNGS | Spectral gamma ray | 15 | 51 |
| | APS | Porosity | 5 and 15 | 43 |
| | HLDT | Bulk density | 2.5 | 38 |
| | DIT-E | Resistivity | 15 | 76/150/200 |
| | TAP | Temperature | 1 per s | NA |
| | | Tool acceleration | 4 per s | NA |
| | | Pressure | 1 per s | NA |
| Formation MicroScanner (FMS)-sonic combination | NGT | Spectral gamma ray | 15 | 46 |
| | GPIT | Tool orientation | 0.25 and 15 | NA |
| | FMS | Microresistivity | 0.25 | 0.5 |
| | DSI/SDT/LSS/BHC | Acoustic velocity | 15 | 107 |

Notes: All tool and tool string names (except the TAP and MGT) are trademarks of Schlumberger. For the complete list of acronyms used in IODP and for additional information about tool physics and use consult IODP-USIO Science Services, LDEO, at **iodp.ldeo.columbia.edu/TOOLS_LABS/tools.html.** * = not included in each logging run. See Table T4 for explanations of acronyms used to describe tool strings and tools. NA = not applicable.

**Table T4.** Acronyms and units for wireline tools.

| Tool | Output | Tool name/Explanation of output | Unit |
|------|--------|----------------------------------|------|
| APS | | Accelerator Porosity Sonde | |
| | APLC | Near array porosity (limestone calibrated) | % |
| | SIGF | Formation capture cross section ($\Sigma f$) | Capture units |
| | STOF | Tool standoff (computed distance from borehole wall) | inch |
| DIT-E | | Dual Iduction Tool | |
| | IDPH | Deep induction resistivity | $\Omega \cdot m$ |
| | IMPH | Medium induction resistivity | $\Omega \cdot m$ |
| | SFLU | Spherically focused resistivity | $\Omega \cdot m$ |
| DSI | | Dipole Sonic Imager | |
| | DTCO | Compressional wave delay time ($\Delta t$) | ms/ft |
| | DTSM | Shear wave delay time ($\Delta t$) | ms/ft |
| | DTST | Stoneley wave delay time ($\Delta t$) | ms/ft |
| FMS | | Formation MicroScanner | |
| | C1, C2 | Orthogonal hole diameters | inch |
| | P1AZ | Pad 1 azimuth | Degrees |
| | | Spatially oriented resistivity images of borehole wall | |
| GPIT | | General Purpose Inclinometer Tool | |
| | DEVI | Hole deviation | Degrees |
| | HAZI | Hole azimuth | Degrees |
| | $F_x, F_y, F_z$ | Earth's magnetic field (three orthogonal components) | Oersted |
| | $A_x, A_y, A_z$ | Acceleration (three orthogonal components) | $m/s^2$ |
| HLDT | | Hostile Environment Litho-Density Tool | |
| | RHOM | Bulk density | $g/cm^3$ |
| | PEFL | Photoelectric effect | $b/e^-$ |
| | LCAL | Caliper (measure of borehole diameter) | inch |
| | DRH | Bulk density correction | $g/cm^3$ |
| HNGS | | Hostile Environment Gamma Ray Sonde | |
| | HSGR | Standard (total) gamma ray | gAPI |
| | HCGR | Computed gamma ray (HSGR minus uranium contribution) | gAPI |
| | HFK | Potassium | wt% |
| | HTHO | Thorium | ppm |
| | HURA | Uranium | ppm |
| NGT | | Natural Gamma Ray Spectrometry Tool | |
| | SGR | Standard total gamma ray | gAPI |
| | CGR | Computed gamma ray (SGR minus uranium contribution) | gAPI |
| | POTA | Potassium | wt% |
| | THOR | Thorium | ppm |
| | URAN | Uranium | ppm |
| MGT | | Multi-Sensor Spectral Gamma Ray Tool | |
| | GR | Total gamma ray | gAPI |
| TAP | | Temperature/Acceleration/Pressure tool | $°C, m/s^2$, psi |

Notes: All tool and tool string names (except the TAP and MGT) are trademarks of Schlumberger. For the complete list of acronyms used in IODP and for additional information about tool physics and use, consult IODP-USIO Science Services, LDEO, at **iodp.ldeo.columbia.edu/ TOOLS_LABS/tools.html.**